Directed evolution of the rRNA methylating enzyme Cfr reveals molecular basis of antibiotic resistance

Short title: Directed evolution of the Cfr resistance enzyme

Kaitlyn Tsai[1], Vanja Stojković[1], Lianet Noda-Garcia[2], Iris D. Young[3], Alexander G. Myasnikov[4], Jordan Kleinman[1], Ali Palla[1], Stephen N. Floor[5,6], Adam Frost[4,7], James S. Fraser[3,7], Dan S. Tawfik[2], Danica Galonić Fujimori[1,7,8]*

[1]Department of Cellular and Molecular Pharmacology; University of California San Francisco; San Francisco, CA 94158, USA.

[2]Department of Biomolecular Sciences, Weizmann Institute of Science; Rehovot, Israel.

[3]Department of Bioengineering and Therapeutic Sciences, University of California San Francisco; San Francisco, CA 94158, USA.

[4]Department of Biochemistry and Biophysics, University of California San Francisco; San Francisco, CA 94158, USA.

[5]Department of Cell and Tissue Biology, University of California San Francisco; San Francisco, CA 94143, USA.

[6]Helen Diller Family Comprehensive Cancer Center, University of California San Francisco; San Francisco, CA 94143, USA.

[7]Quantitative Biosciences Institute, University of California San Francisco; San Francisco, CA 94158, USA.

[8]Department of Pharmaceutical Chemistry, University of California San Francisco; San Francisco, CA 94158, USA.

*Corresponding author. Email: Danica.Fujimori@ucsf.edu

ABSTRACT

Alteration of antibiotic binding sites through modification of ribosomal RNA (rRNA) is a common form of resistance to ribosome-targeting antibiotics. The rRNA-modifying enzyme Cfr methylates an adenosine nucleotide within the peptidyl transferase center, resulting in the C-8 methylation of A2503 (m^8A2503). Acquisition of *cfr* results in resistance to eight classes of ribosome-targeting antibiotics. Despite the prevalence of this resistance mechanism, it is poorly understood whether and how bacteria modulate Cfr methylation to adapt to antibiotic pressure. Moreover, direct evidence for how m^8A2503 alters antibiotic binding sites within the ribosome is lacking. In this study, we performed directed evolution of Cfr under antibiotic selection to generate Cfr variants that confer increased resistance by enhancing methylation of A2503 in cells. Increased rRNA methylation is achieved by improved expression and stability of Cfr through transcriptional and post-transcriptional mechanisms, which may be exploited by pathogens under antibiotic stress as suggested by natural isolates. Using a variant which achieves near-stoichiometric methylation of rRNA, we determined a 2.2 Å cryo-EM structure of the Cfr-modified ribosome. Our structure reveals the molecular basis for broad resistance to antibiotics and will inform the design of new antibiotics that overcome resistance mediated by Cfr.

KEY WORDS: Cfr; directed evolution; antibiotic resistance; RNA modification; 23S rRNA; peptidyl transferase center; cryo-EM structure

INTRODUCTION

A large portion of clinically-relevant antibiotics halt bacterial growth by binding to the ribosome and inhibiting protein synthesis (Arenz and Wilson, 2016; Tenson and Mankin, 2006; Wilson, 2009). Since antibiotic binding sites are primarily composed of ribosomal RNA (rRNA), rRNA-modifying enzymes that alter antibiotic binding pockets are central to evolved resistance (Vester and Long, 2013; Wilson, 2014). The rRNA-methylating enzyme Cfr modifies an adenosine nucleotide located within the peptidyl transferase center (PTC), a region of the ribosome essential for catalyzing peptide bond formation and consequently, a common target for antibiotics (Kehrenberg et al., 2005; Schwarz et al., 2000). Cfr is a radical SAM enzyme that methylates the C8 carbon of adenosine at position 2503 (m^8A2503, *E. coli* numbering) (Giessing et al., 2009; Grove et al., 2011b; Kaminska et al., 2010; Yan et al., 2010; Yan and Fujimori, 2011). Due to the proximal location of A2503 to many antibiotic binding sites, introduction of a single methyl group is sufficient to cause resistance to eight classes of antibiotics simultaneously: **ph**enicols, **l**incosamides, **o**xazolidinones, **p**leuromutilins, **s**treptogramin **A** ($PhLOPS_A$), in addition to nucleoside analog A201A, hygromycin A, and 16-membered macrolides (Long et al., 2006; Polikanov et al., 2015; Smith and Mankin, 2008). Among rRNA modifying enzymes, this extensive cross-resistance phenotype is unique to Cfr and presents a major clinical problem.

Cfr emergence in human pathogens appears to be a recent event, with the first case reported in 2007 from a patient-derived *Staphylococcus aureus* isolate (Arias et al., 2008; Toh et al., 2007). Since then, the *cfr* gene has been identified across the globe in both gram-positive and gram-negative bacteria (Shen et al., 2013; Vester, 2018), and has been associated with several clinical resistance outbreaks to the oxazolidinone antibiotic, linezolid (Bonilla et al., 2010; Cai et al., 2015; Dortet et al., 2018; Layer et al., 2018; Lazaris et al., 2017; Locke et al., 2010; Morales et al., 2010; Weßels et al., 2018). The vast spread of Cfr is attributed to its association with mobile genetic elements and relatively low impact on bacterial fitness, suggesting that *cfr* can be rapidly disseminated within bacterial populations (LaMarre et al., 2011; Schwarz et al., 2016).

Due to the ability of Cfr to confer resistance to several antibiotics simultaneously, it is critical to understand how bacteria may adapt under antibiotic pressure to enhance Cfr activity and bolster protection against ribosome-targeting molecules. Identification of Cfr mutations that improve resistance will also be critical for informing clinical surveillance and designing strategies to counteract resistance. A major limitation in our current understanding of Cfr-mediated resistance is the lack of structural

insight into changes in the ribosome as a result of Cfr modification. Steric occlusion of antibiotic binding has been proposed as a model to rationalize altered antibiotic susceptibility (Polikanov et al., 2015). Additionally, the observation that A2503 can adopt both *syn* and *anti*-conformations in previously reported ribosome structures suggests that methylation may regulate conformation of the base, as previously proposed (Schlünzen et al., 2001; Stojković et al., 2020; Toh et al., 2008; Tu et al., 2005). However, direct evidence for how m^8A2053 alters antibiotic binding sites to inform the design of next-generation molecules that can overcome Cfr resistance is lacking.

In this study, we identified mechanisms that enhance antibiotic resistance by performing directed evolution of a *cfr* found in a clinical MRSA isolate under antibiotic selection (Barlow and Hall, 2003). The obtained highly resistant Cfr variants show increased rRNA methylation, driven primarily by robust improvements in Cfr cellular levels, achieved either by higher transcription or increased translation and improved cellular stability. In particular, mutation of the second Cfr amino acid to lysine strongly enhances translation and resistance. Lastly, we used an evolved variant which achieves near-stoichiometric rRNA methylation to generate a high-resolution cryo-EM structure of the Cfr-modified *E. coli* ribosome. The obtained structural insights provide a rationale for how m^8A2503 causes resistance to ribosome antibiotics.

RESULTS

Evolved Cfr variants confer enhanced antibiotic resistance

To perform directed evolution of Cfr, we used error-prone PCR (EP-PCR) to randomly introduce 1-3 mutations into the *cfr* gene obtained from a clinical MRSA isolate (Toh et al., 2007), herein referred to as CfrWT (**Fig. 1a**). Mutagenized *cfr* sequences were then cloned into a pZA vector where Cfr was expressed under tetracycline-inducible promoter P_{tet} introduced to enable precise control of Cfr expression (Wellner et al., 2013). The resulting library of ~10^7 *E. coli* transformants was selected for growth in the presence of increasing amounts of tiamulin, a pleuromutilin antibiotic to which Cfr confers resistance. During each round, a subset of the surviving colonies was sequenced to identify new mutations. After two rounds of evolution, *wild-type* Cfr was no longer detected, indicating that the introduced mutations provide enhanced survivability in the presence of tiamulin. After five rounds of

mutation and selection, we performed two rounds of selection without mutagenesis, and with high tiamulin concentrations, thus leading to fixation of mutations that provide robust resistance.

Analysis of surviving *cfr* sequences from the final rounds of selection revealed notable trends (**Supplementary Table 2**). Three positions were primarily mutated: N2, I26, and S39. By homology modeling, these mutational hotspots appear distal from the enzyme active site (>12 Å; **Fig. 1b**). Secondly, ~28% of sequences contained alterations to the promoter. These alterations consist of either P_{tet} duplication, or insertion of a partial P_{tet} sequence (**Supplementary Table 3**).

We selected 7 evolved Cfr variants, referred herein as CfrV1-V7, as representative mutational combinations for further characterization (**Fig. 1c**). All selected Cfr variants contain mutations in the *cfr* open reading frame while CfrV6 and CfrV7 also harbor P_{tet} alterations (**Fig. 1d**). Compared to CfrWT, these variants confer ~2 to ~16-fold enhanced resistance to $PhLOPS_A$ antibiotics, yet with no changes in susceptibility to trimethoprim, an antibiotic that does not inhibit the ribosome (**Fig. 1e, Supplementary Table 4)**. Interestingly, the promoter alterations enable CfrV7 to be expressed and confer resistance to tiamulin in the absence of inducer (**Supplementary Fig. 1**). The robustness of resistance, and the absence of active-site mutations, suggests Cfr variants do not act as dominant-negative enzymes that inhibit C-2 methylation of A2503, as observed in a previous directed evolution experiment (Stojković et al., 2016). Furthermore, the specificity of resistance to $PhLOPS_A$ antibiotics suggests that these Cfr variants elicit their effects through PTC modification rather than triggering a stress response that confers global resistance.

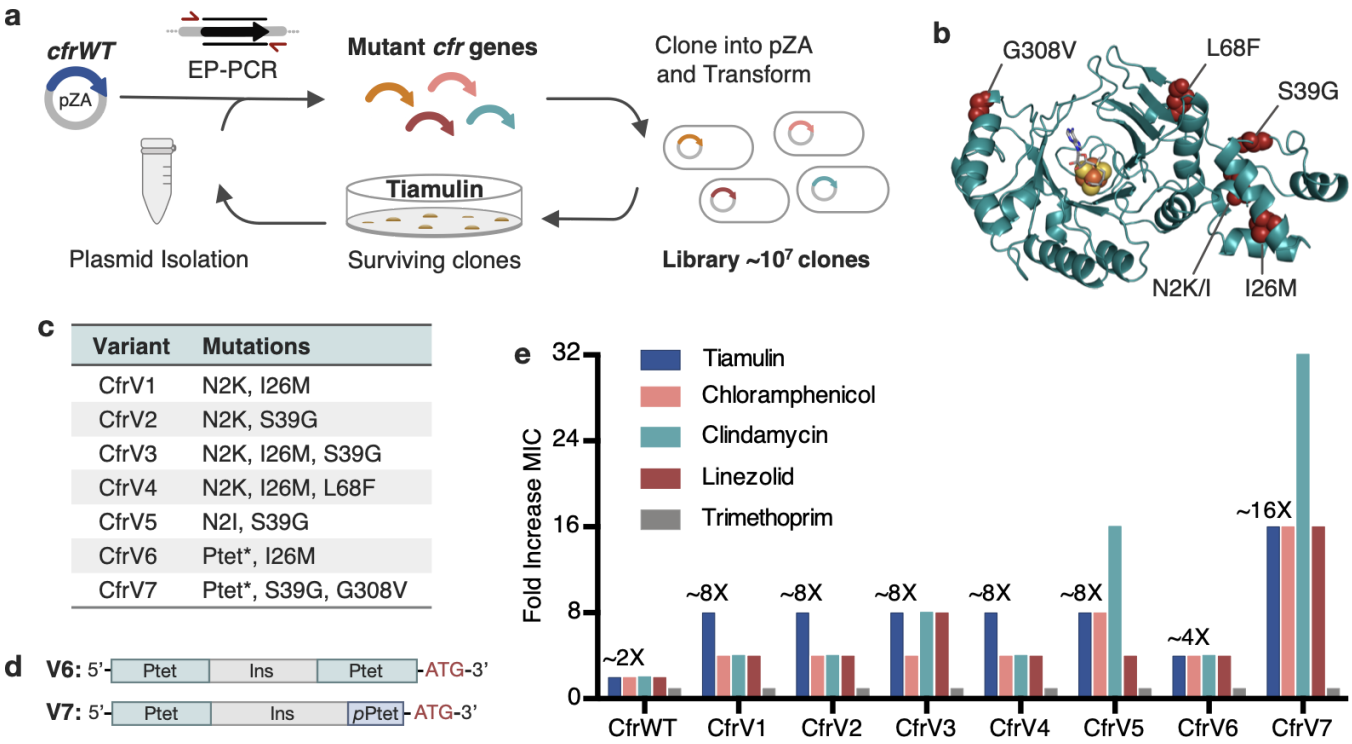

Fig. 1. Evolved variants of Cfr exhibit improved resistance to PhLOPS$_A$ ribosome antibiotics. (**a**) Evolution of Cfr under selection by the PTC-targeting antibiotic tiamulin. (**b**) Cfr homology model based on RlmN generated by I-TASSER server (Yang and Zhang, 2015) with mutagenic hotspots in red. Active site denoted by *S*-adenosylmethionine (grey) and [4Fe-4S] cluster (orange). (**c**) Evolved variants containing Cfr mutations selected for further study. Ptet* indicates alterations to promoter sequence. **(d)** Promoter architecture of CfrV6 and CfrV7 where *p*Ptet designates a partial Ptet promoter sequence and Ins designates a variable insertion sequence. (**e**) Fold improvement in MIC resistance value for PhLOPS$_A$ antibiotics and trimethoprim compared to empty pZA vector control determined from three biological replicates. Trimethoprim is a negative control antibiotic that does not target the ribosome. Numerical MIC values displayed in **Supplementary Table 4**.

Variants exhibit increased rRNA methylation and Cfr protein levels

To test the hypothesis that Cfr variants mediate higher resistance by increasing the fraction of ribosomes with m^8A2503, we evaluated the methylation status of A2503 by mass spectrometry. Specifically, we expressed Cfr in *E. coli* and used oligonucleotide protection to isolate a 40-nt fragment of 23S rRNA containing A2503. The isolated fragment was then enzymatically digested and analyzed by MALDI-TOF mass spectrometry (**Fig. 2a, Supplementary Fig. 2**). As expected, an empty vector produces a 1013 m/z fragment corresponding to the mono-methylated m^2A2503, modification installed by the endogenous enzyme RlmN. Upon expression of Cfr, we observe a reduction in the 1013 m/z peak and the emergence of a new peak at 1027 m/z, corresponding to m^2A2503 conversion into hypermethylated m^2m^8A2503. CfrWT is able to convert less than ~40% of m^2A2503 into the hypermethylated m^2m^8A2503 product. In contrast, the evolved variants achieve ~50-90% methylation of A2503, indicating that variants are more active than CfrWT *in vivo*.

The ability of evolved Cfr variants to achieve enhanced ribosome methylation *in vivo* could be attributed to enhanced enzymatic activity and/or higher levels of functional enzyme. To test the hypothesis that Cfr variants achieve higher turnover number, we anaerobically purified and reconstituted CfrWT and a representative evolved variant, CfrV4. We then evaluated the ability of CfrWT and CfrV4 to methylate a 23S rRNA fragment (2447-2625) *in vitro* by monitoring the incorporation of radioactivity from [^{3}H-methyl] *S*-adenosylmethionine (SAM) into RNA substrate under saturating conditions (Bauerle et al., 2018). However, no significant difference in k_{cat} between CfrWT ($3.45 \times 10^{-2} \pm 3.2 \times 10^{-3}$ min^{-1}) and CfrV4 ($2.25 \times 10^{-2} \pm 1.3 \times 10^{-3}$ min^{-1}) was observed (**Supplementary Fig. 3**).

Given these findings, we hypothesized that the variants might alter protein levels. To monitor Cfr protein levels, we inserted a flexible linker followed by a C-terminal FLAG tag, which does not alter resistance (**Supplementary Table 5**). Interestingly, immunoblotting against FLAG revealed that in addition to full-length Cfr, N-terminally truncated Cfr proteins are also produced (**Fig. 2b**). The truncations result from translation initiation at internal methionines but do not contribute to resistance (**Supplementary Fig. 4**), indicating that they are non-functional enzymes unable to methylate A2503. Interestingly the larger molecular weight truncation is present only in CfrV1/V4/V6 and is generated by the I26M mutation introduced during directed evolution. Quantification of resistance-causative, full-length Cfr proteins alone revealed that the evolved variants achieve ~20-100-fold higher steady-state protein levels than CfrWT (**Fig. 2b**).

We measured transcript levels for all variants to assess the contribution of altered transcription to increased protein levels. For Cfr variants with promoter alterations, enhanced production of the Cfr transcript is a large contributor to Cfr protein expression, as CfrV6 and CfrV7 exhibit ~6 and ~10-fold enhancement in Cfr mRNA levels compared to CfrWT, respectively (**Fig. 2c**). However, the ~2 to 3-fold increase in mRNA levels for CfrV1-5 cannot explain the multi-fold improvement in protein expression and indicates that these variants also boost protein production through a post-transcriptional process. This is further supported by the expression profiles for CfrV1-5, which are dominated by the full-length protein (**Fig. 2d**). Interestingly, enhanced production of Cfr protein correlates with larger fitness defects in *E. coli*, with an increase in doubling time of ~4 min for CfrV7 compared to empty vector in the absence of antibiotics (**Fig. 2e**).

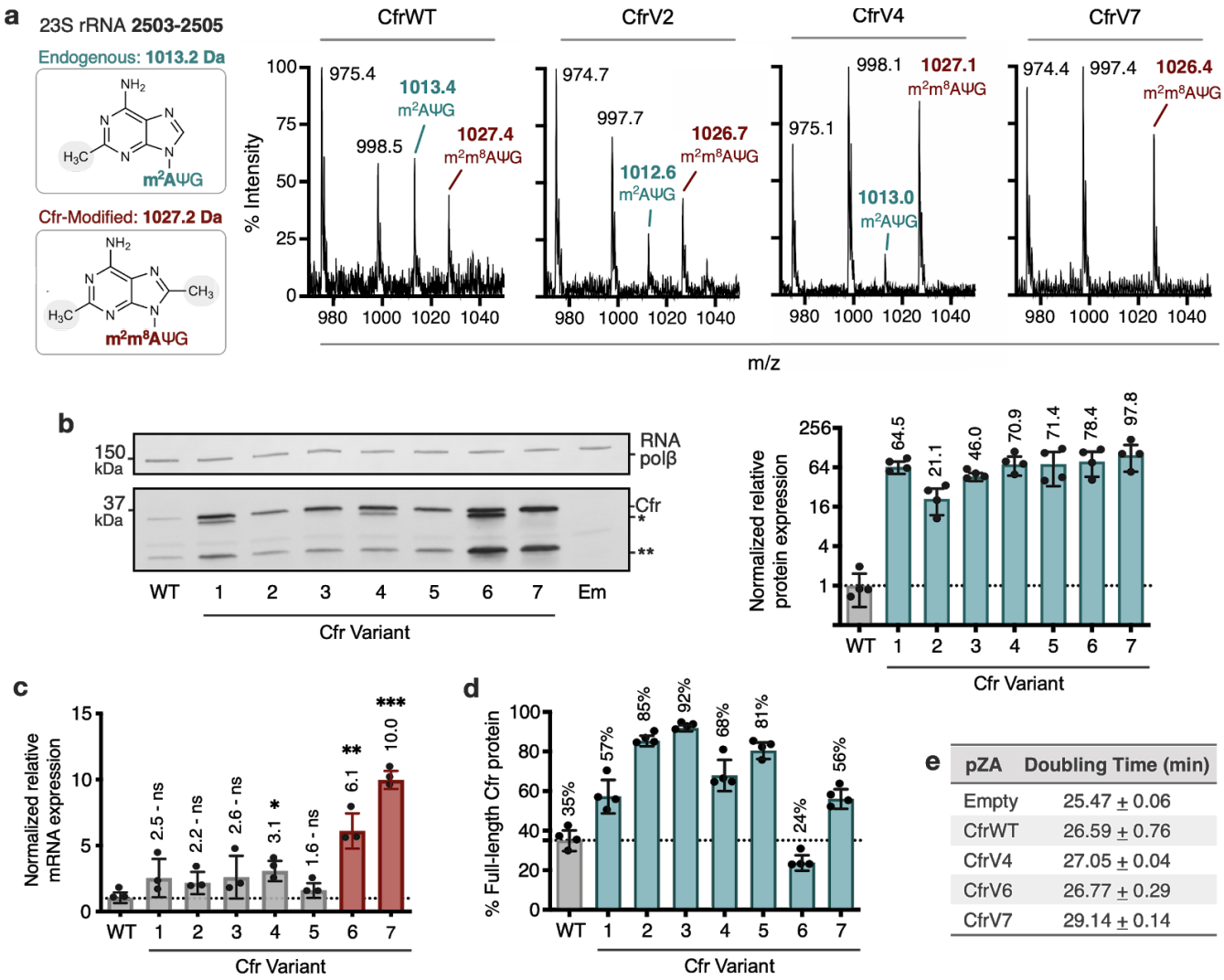

Fig. 2. Cfr variants cause increased methylation of 23S rRNA at A2503, correlating with enhanced production of Cfr protein. (**a**) Endogenously modified (m^2A2503) and Cfr-hypermodified (m^2m^8A2503) rRNA fragments correspond to m/z values of 1013 and 1027, respectively. MALDI-TOF mass spectra of 23S rRNA fragments isolated from *E. coli* expressing CfrWT, and evolved Cfr variants V2, V4, and V7. Ψ is pseudouridine, m^2A is 2-methyladenosine, is m^2m^8A is 2,8-dimethyladenosine. (**b**) Relative protein expression of full-length Cfr variants compared to full-length CfrWT detected by immunoblotting against a C-terminal FLAG tag and quantification of top Cfr bands. Signal was normalized to housekeeping protein RNA polymerase β-subunit. Data is presented as the average of four biological replicates with standard deviation on a $\log_2$ axis. Asterisks denote N-terminally truncated versions of Cfr that do not contribute to resistance. Em = empty vector control. (**c**) Relative transcript levels for variants compared to CfrWT determined from three biological replicates with standard deviation. (**d**) Percentage of total Cfr expression attributed to production of full-length Cfr protein, presented as the average of four biological replicates with standard deviation. (**e**) Doubling times for *E. coli* expressing empty plasmid, CfrWT, or Cfr variants determined from three biological replicates with standard error.

Promoter and second position mutations drive Cfr resistance

Given that the evolved variants achieve robust enhancement in Cfr expression we sought to elucidate the mechanism(s) by which this occurs. To evaluate the importance of promoter alterations, we generated a construct where the P_{tet}* promoter sequence from CfrV6 was inserted upstream of CfrWT open reading frame, herein referred to as P_{tet}*V6-CfrWT. The insertion of P_{tet}* alone was sufficient to elicit improvement in Cfr expression (**Fig. 3a**). Furthermore, *E. coli* expressing P_{tet}*V6-CfrWT resembled CfrV6 in its ability to survive in the presence of chloramphenicol (**Fig. 3b**). Together, these results suggest the altered promoter drives expression and resistance for CfrV6.

To investigate the contributions of mutations within the Cfr protein, we generated constructs containing Cfr mutations N2K/I, I26M, and S39G in isolation. Interestingly, we observe that mutations at the second position, N2K and N2I, display the largest enhancements in expression, ~27-fold and ~12-fold respectively (**Fig. 3a**). The dominance of the second position mutants is further manifested in *E. coli* expressing CfrN2K, but not I26M or S39G, exhibiting similar survival in the presence of chloramphenicol to that of the triple mutant, CfrV3 (**Fig. 3c**). Similarly, *E. coli* expressing CfrN2I also exhibits increased resistance to chloramphenicol when compared to the corresponding directed evolution variant, CfrV5, albeit weaker than CfrN2K (**Supplementary Fig. 5a**). Together, these results suggest that the second position mutations drive the robust expression and resistance observed for CfrV1-5. Of note, ribosome methylation by the produced Cfr does not impact the translation of CfrN2K, as this mutant and its corresponding catalytically inactive double mutant protein CfrN2K_C338A are similarly highly expressed (**Supplementary Fig. 5b-c**).

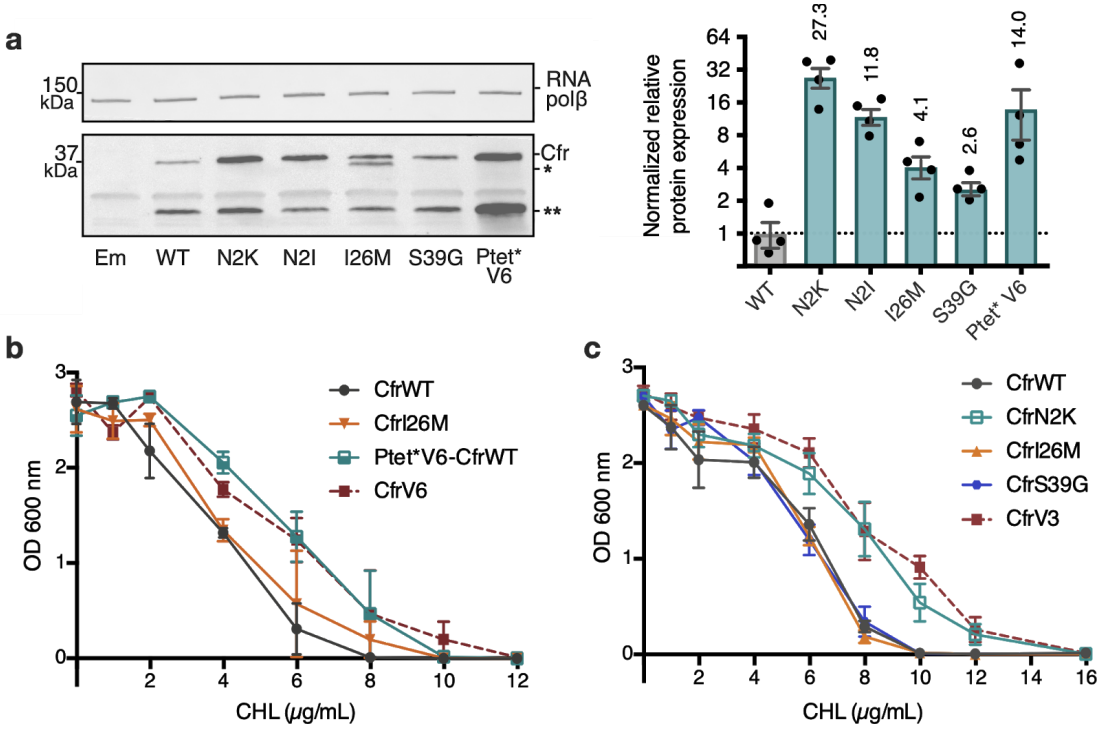

Fig. 3. Mutations to the second amino acid and promoter are the largest contributors to Cfr expression and resistance. (**a**) Effect of Cfr mutations and promoter alteration on relative Cfr protein expression was assessed by immunoblotting against a C-terminal FLAG tag. Quantification was performed for full-length Cfr protein normalized to housekeeping protein RNA polymerase β-subunit. Data is presented as the average of four biological replicates with standard deviation on a $\log_2$ axis. Asterisks denote N-terminally truncated Cfr protein products that do not contribute to resistance and were not included in quantification. Em = empty vector control. (**b**) and (**c**) Dose-dependent growth inhibition of *E. coli* expressing pZA-encoded CfrWT, CfrV6 (panel b), CfrV3 (panel c) and individual mutants that comprise these variants towards chloramphenicol (CHL) presented as an average of three biological replicates with standard error.

Mutations impact Cfr translation and degradation

The Cfr coding mutations drive enhanced steady-state protein levels of Cfr protein through a post-transcriptional process. However, because levels at steady-state reflect the net effect of protein synthesis and degradation, we sought to evaluate how Cfr mutations impact both processes, especially since the nature of N-terminal amino acids and codons can greatly influence both translation and degradation in bacteria (Bentele et al., 2013; Bhattacharyya et al., 2018; Boël et al., 2016; Goodman et al., 2013; Gottesman, 2003; Looman et al., 1987; Sato et al., 2001; Stenström et al., 2001a, 2001b; Stenström and Isaksson, 2002; Tuller et al., 2010a; Verma et al., 2019).

To test the hypothesis that second position mutations enhance translation of mutants, we used polysome profiling to evaluate the relative abundance of Cfr mRNA in polysome fractions. Polysome profiles derived from 10-55% sucrose gradients appear similar across biological conditions, suggesting expression of CfrWT and its evolved mutants do not affect global translation (**Fig. 4a-b**). CfrWT transcripts migrate with low polysomes (fractions 10, 11) (**Fig. 4c**). In contrast, CfrV4 transcripts are strongly shifted toward high polysomes (fractions 16, 17), which indicate that CfrV4 mRNA is associated with a large quantity of ribosomes and is better translated than CfrWT (**Fig. 4d**). Further support that CfrV4 is well-translated is the observation that CfrV4 mRNA co-migrates with mRNA of the well-translated housekeeping gene, *recA (Li et al., 2014)* (**Supplementary Fig. 6a-c**). At least in part, this is due to the N2K mutation which shifts transcripts to higher polysomes fractions (fractions 12, 13) (**Fig. 4c**). The *recA* control mRNA shows excellent reproducibility across biological samples, indicating that the observed shift of mutant Cfr transcripts towards higher polysomes is due to introduced mutations (**Fig. 4b**). Taken together, these results suggest that enhanced translation is a cumulative effect of N2K and other ORF mutations obtained by directed evolution.

To further interrogate the role of second position mutations in Cfr translation, we determined the second codon identity for all sequenced variants from the final rounds of evolution (**Supplementary Table 2**). Interestingly, all N2K mutations were encoded by an AAA codon, while AUU encoded all N2I mutations. In *E. coli*, the tRNA molecules that decode K(AAA) and I(AUU) are slightly more abundant than the wild-type N(AAU), accounting for 3.0% and 5.4% of the tRNA pool compared to 1.9%, respectively (Dong et al., 1996). To test if tRNA abundance and codon sequence contribute to enhanced translation, we evaluated the impact of synonymous codons on protein expression. Lysine codons AAA and AAG are decoded by the same $tRNA^{Lys}$ in *E. coli*. Interestingly, mutating CfrN2K from AAA to

AAG, which increases G/C content, did not significantly impact expression (**Supplementary Fig. 6d**). The isoleucine AUA codon is decoded by the low-abundant $tRNA^{Ile2}$ (Del Tito et al., 1995; Nakamura et al., 2000). Mutation of N2I from AUU to the AUA rare codon resulted in a ~2-fold decrease in Cfr expression, supporting tRNA abundance as a contributing factor (**Supplementary Fig. 6d**).

To evaluate impact of mutations introduced during directed evolution on protein half-life, we monitored changes in protein abundance over time after halting expression with rifampicin (**Fig. 4e, Supplementary Fig. 7**). While CfrWT is rapidly degraded with a half-life of ~20 min, CfrN2K/I exhibit increased half-lives of ~60 min. These results suggest that mutation of the second amino acid to lysine or isoleucine contribute to improved steady-state expression both by enhancing translation and stability of Cfr in the cell. CfrS39G also exhibits an increased half-life of ~60 min. The half-life increase is the most pronounced for the I26M single point mutant and similar to that of the triple-mutant, CfrV3 (>100 min for both proteins). Together, these results suggest that evolved variants achieve higher expression through mutations that both enhance translation and decrease degradation of mutant Cfr proteins.

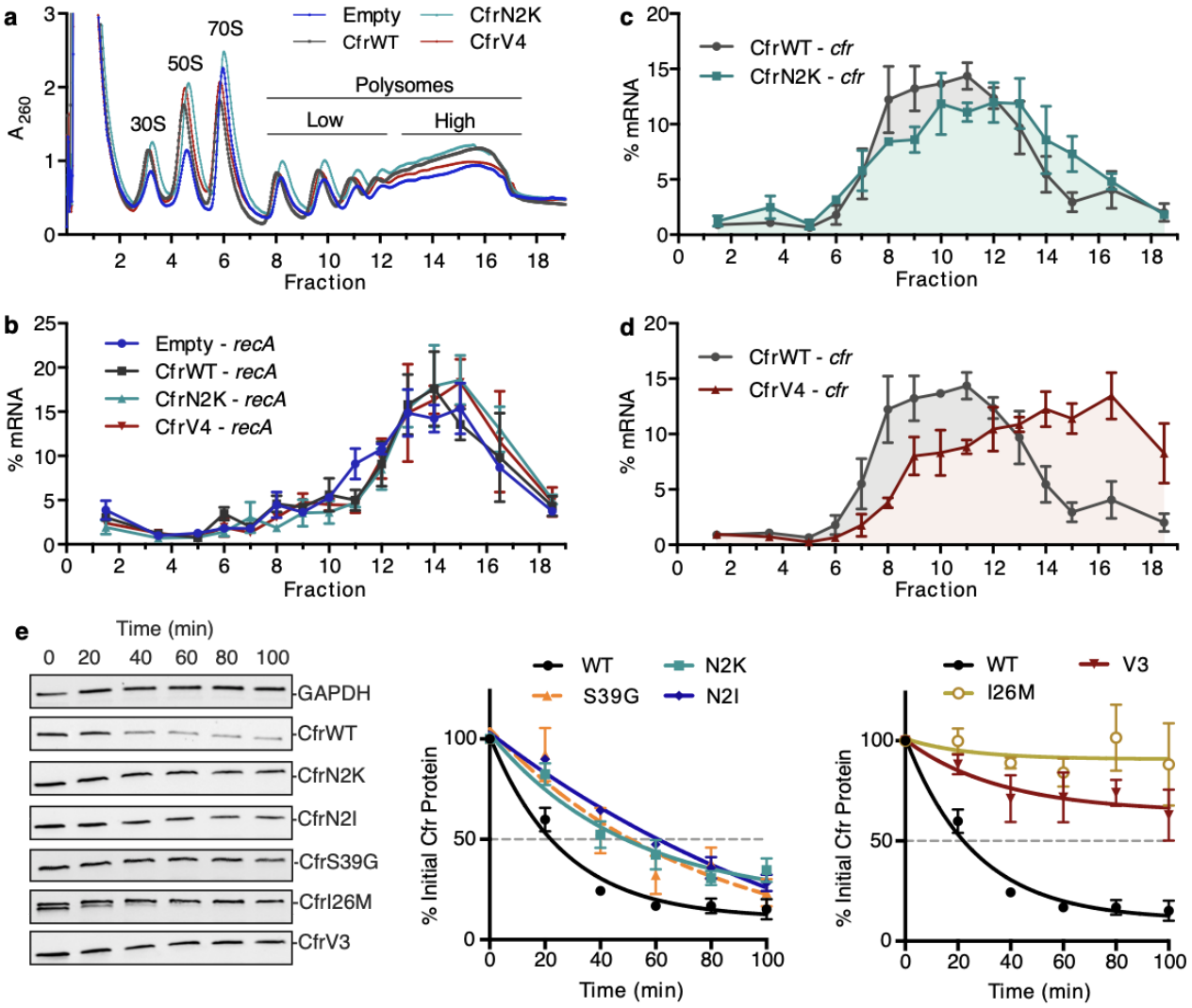

Fig. 4. Directed evolution mutations impact Cfr translation and degradation. (**a**) Sucrose gradient fractionation of polysomes from *E. coli* expressing empty vector or CfrWT/N2K/V4 denoting fractions corresponding to low- and high-density polysomes. (**b**) mRNA distribution of well-translated, housekeeping gene *recA* across polysome profiles. (**c**) mRNA distribution of Cfr transcripts expressing CfrWT or CfrN2K. (**d**) mRNA distribution of Cfr transcripts expressing CfrWT or CfrV4. For B-D, transcript levels for each fraction were determined by RT-qPCR and normalized by a luciferase mRNA control spike-in. Values presented as the average of three biological replicates with standard error. (**e**) Protein degradation kinetics of CfrWT, single mutations CfrN2K/N2I/S39G/I26M, and evolved variant CfrV3 in *E. coli* after halting expression by rifampicin treatment. Percentage of Cfr protein remaining over time was determined by immunoblotting against C-terminal FLAG tag and presented as the average of three biological replicates with standard error.

Evolved Cfr enables understanding of the structural basis of resistance

Molecular understanding of Cfr-mediated resistance to antibiotics necessitates structural insights into methylated ribosomes. However, obtaining the structure of Cfr-modified ribosome has been so far hampered by moderate methylation efficiency of *S. aureus* Cfr, a challenge that can be addressed by the improved methylation ability of directed evolution variants. Of all characterized evolved variants, CfrV7 achieves the highest levels of antibiotic resistance and methylation of rRNA, providing a unique tool for structural determination. Relative peak quantification of the MALDI spectra revealed that CfrV7 achieved near-stoichiometric (~90%) m^8A2503 methylation (**Supplementary Fig. 2**).

Ribosomes were purified from *E. coli* expressing CfrV7 to obtain a 2.2 Å cryo-EM structure of the Cfr-modified 50S ribosomal subunit (**Fig. 5a, Supplementary Fig. 8, Supplementary Table 6**). The high resolution cryo-EM density map enabled modeling all known modified nucleotides including the novel C8 methylation of A2503 (**Fig. 5b**). Furthermore, comparison of the Cfr-modified ribosome with the high resolution cryo-EM structure of unmodified, *wild-type* ribosome we published previously (Stojković et al., 2020) allowed us to identify with high confidence any structural changes due to the presence of m^8A2503. Importantly, modification of A2503 by Cfr does not affect the conformation or position of the A2503 nucleotide. The adenine ring remains in the *syn*-conformation and places the newly installed C8-methyl group directly into the PTC to sterically obstruct antibiotic binding (**Fig. 5c-d**).

Strikingly, beyond the addition of a single methyl group to the substrate nucleotide, presence of m^8A2503 does not result in any additional structural changes to the PTC region of the ribosome (**Fig. 5c**). Furthermore, the increased resistance provided by CfrV7 appears to be mediated specifically by improved methylation of A2503. No off-target activity of the evolved variant was observed as manual inspection did not reveal density that could correspond to additional C8-methyl adenosines within the high-resolution regions of the 50S ribosomal subunit. This result was cross-validated using our qPTxM tool (Stojković et al., 2020), which identified only A2503 and A556 as possible C8-methyl adenosines. Closer examination of A556 reveals it registered as a false positive (**Supplementary Fig. 9a-d**).

Contrary to previous reports, we do not observe changes to methylation of C2498, a distal PTC nucleotide whose endogenous 2'-O-ribose modification has previously been reported to be suppressed by Cfr methylation of A2503 and hypothesized to alter the PTC through long-range effects (Giessing et

al., 2009; Kehrenberg et al., 2005; Purta et al., 2009). Although it is unclear what percentage of C2498 retains the native modification in our structure, we observe clear density for the methyl group and the nucleotide conformation is unaltered. The density for the methyl group is slightly off of the rotameric position, but the dropoff in density along the methyl bond matches the expected shape (**Supplementary Fig. 9e-g**). Together, the results do not indicate that conformational changes to C2498 are involved in Cfr-mediated resistance.

Structural superposition of the Cfr-modified ribosome with ribosomes in complex with $PhLOPS_A$ antibiotics enables direct identification of chemical moieties responsible for steric collision with m^8A2503 for these five antibiotic drug classes (**Supplementary Fig. 10**). For example, overlay of a bacterial ribosome in complex with the pleuromutilin derivative tiamulin, the selection antibiotic used during directed evolution, reveals steric clashes between the C10 and C11 substituents of the antibiotic with the Cfr-introduced methyl group (**Fig. 5d**). The pleuromutilin class of antibiotics have recently regained interest for their applications as antimicrobial agents in humans but existing molecules remain ineffective against pathogens with Cfr (Goethe et al., 2019). Given recent synthetic advances that enable more extensive modification of the pleuromutilin scaffold (Farney et al., 2018; Murphy et al., 2017), the structural insights we obtained will inform the design of next-generation antibiotics that can overcome Cfr-mediated resistance.

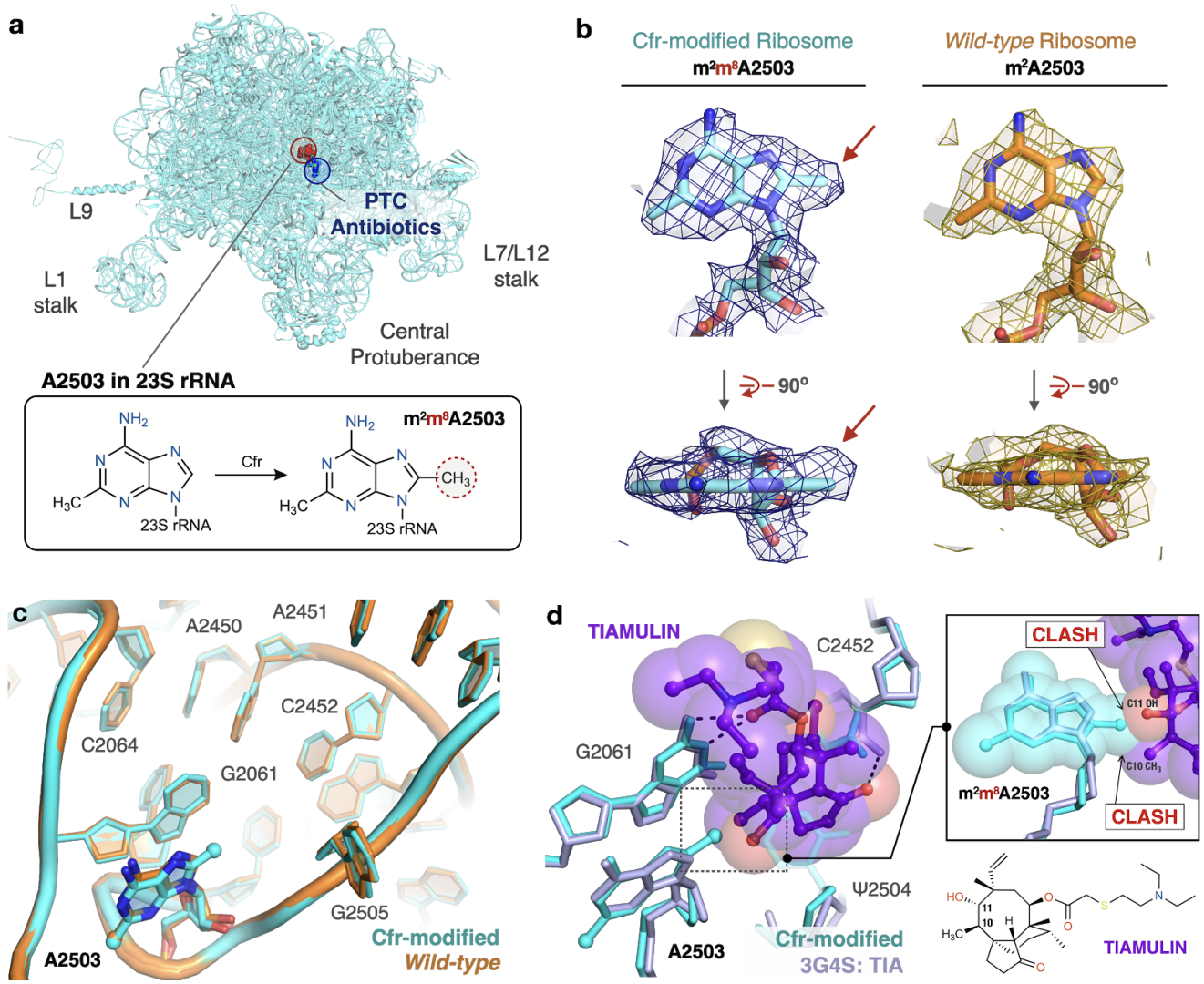

Fig. 5. Near-stoichiometric ribosome methylation by CfrV7 enables structural understanding of Cfr-mediated resistance to antibiotics. (**a**) Cfr-modified 50S ribosomal subunit highlighting adenosine 2503 (A2503) within 23S rRNA and the binding site of PTC-targeting antibiotics. Cfr methylates A2503 at the C8 carbon to produce m^2m^8A2503. (**b**) Cryo-EM density maps of adenosine 2503 in 23S rRNA contoured to 3σ. Cfr-modified (m^2m^8A2503) in cyan. *Wild-type* (m^2A2503) in orange; PDB 6PJ6. (**c**) Close up view of 23S rRNA nucleotides in the 50S ribosomal subunit. Cfr-modified ribosome in cyan. *Wild-type* ribosome in orange; PDB 6PJ6. (**d**) Structural overlay of Cfr-modified ribosome (cyan) and *H. marismortui* 50S ribosome in complex with pleuromutilin antibiotic tiamulin (purple, PDB 3G4S) highlighting steric clashes between m^8A2503 and the antibiotic.

DISCUSSION

By relying on directed evolution under antibiotic selection, we identified strategies that increase the ability of a multi-antibiotic resistance determinant Cfr to cause resistance. Enhanced resistance is associated with improved *in vivo* methylation of rRNA at C8 position of A2503. The positive correlation between extent of rRNA modification and resistance aligns with previous studies that investigated linezolid resistance caused by mutation of rRNA, where the severity of linezolid resistance was proportional to the number of 23S rRNA alleles harboring the resistance mutation (Besier et al., 2008; Ebihara et al., 2014; Lobritz et al., 2003). While alteration of the antibiotic binding site through mutations and enzymatic modification of 23S rRNA are functionally distinct, dependence on the extent of rRNA modification provides parallels between the two mechanisms. Although Cfr-mediated methylation is an enzymatic process, the ability of Cfr to confer resistance is restricted by ribosome assembly. Since the A2503 is only accessible to Cfr prior to incorporation of 23S rRNA into the large ribosomal subunit (Yan et al., 2010), the extent of resistance correlates with the ability of the enzyme to methylate 23S rRNA prior to its incorporation into the 50S subunit. The results of our evolution experiment indicate that increasing the intracellular concentrations of Cfr, rather than improving catalysis of an enzyme with a complex radical mechanism (Bauerle et al., 2018; Grove et al., 2011a; McCusker et al., 2012; Yan and Fujimori, 2011) is the preferred strategy to increase the proportion of ribosomes with the protective m^8A2503 modification.

The evolved Cfr variants improve expression using two mechanisms. Improved Cfr expression for CfrV6/7 is driven by increased transcription due to alterations to the P_{tet} promoter likely introduced by primer slippage during the error-prone PCR step of directed evolution. CfrV6 contains a full duplication of P_{tet}, providing two sites for transcription initiation, likely responsible for enhanced *cfr* transcript levels. Interestingly, this result parallels a clinical instance of high Cfr resistance discovered in a *S. epidermidis* isolate where transcription of *cfr* was driven by two promoters (LaMarre et al., 2013) and highlights transcriptional regulation as an important mechanism for modulating the *in vivo* activity of Cfr.

Improved expression for evolved variants CfrV1-5 is mediated by mutations that improve both translational efficiency and protein stability *in vivo*. Of the tested mutations, I26M provides the largest improvement in stability. Of note, the N-terminally truncated Cfr derived from translation initiation at I26M is rapidly degraded, as no detectable protein is observed after 60 min (**Fig. 4e**). However, these

results indicate that the costly production and clearance of this nonfunctional protein is offset by the improved cellular stability of the full-length Cfr carrying the I26M mutation.

Of the mutations investigated, N2K is the largest contributor to enhanced Cfr expression and resistance. Although N2K contributes to cellular stability, our results suggest that improved Cfr translation is the dominant role of this mutation. Our results indicate that the effect of N2K on translation may be mediated, at least in part, by tRNA abundance. The influence of N-terminal residues on early stages of translation has been well documented, with several proposed models to explain how tRNA abundance, in addition to local mRNA sequence and structure, amino acid composition of the nascent chain, and interaction between the mRNA or the nascent chain and the ribosome itself influence translation initiation and elongation (Bentele et al., 2013; Bhattacharyya et al., 2018; Boël et al., 2016; Cambray et al., 2018; Goodman et al., 2013; Gorochowski et al., 2015; Kudla et al., 2009; Riba et al., 2019; Tuller et al., 2010a, 2010b; Verma et al., 2019). Although the mechanism is poorly understood, the presence of an AAA lysine codon after the start codon can be associated with improved translation efficiency (Brock et al., 2007; Looman et al., 1987; Sato et al., 2001; Stenström et al., 2001a, 2001b; Stenström and Isaksson, 2002; Zalucki et al., 2007). (Brock et al., 2007; Looman et al., 1987; Sato et al., 2001; Stenström et al., 2001a, 2001b; Stenström and Isaksson, 2002; Zalucki et al., 2007). Interestingly, the observed internal translation start sites (I26M, M95) that are responsible for producing Cfr truncations (**Fig. 2B**, **Supplementary Fig. 4**) contain a lysine immediately after methionine, further highlighting the putative role for lysine codons in early steps of translation.

To date, only a few *S. aureus* Cfr variants have been reported and no mutations matching those obtained from directed evolution have been found in clinical isolates. However, enhanced expression through positioning of Lys as the second amino acid of Cfr can be recapitulated by accessing an upstream translational start site found in a native sequence context of *cfr* (**Supplementary Fig. 11**). In the specific case of the pSCFS1 resistance plasmid, the sequence upstream of the annotated start codon, which we validated as the start site under the experimental conditions tested (**Supplementary Fig. 12**), contains regulatory elements that have been proposed to modulate Cfr expression (Kehrenberg et al., 2007; Schwarz et al., 2000). It is plausible that in response to antibiotics, the upstream start codon is used to add three amino acids (MKE) to the N-terminus of Cfr and thus placement of a lysine (K) at position two of the newly expressed protein, analogous to the N2K mutation. Although start codon selection requires further investigation, N-terminal addition of MKE to Cfr expressed under non-native

P_{tet} promoter phenocopies the N2K directed evolution mutation, resulting in increased expression and resistance compared to CfrWT (**Supplementary Fig. 11**). Since our assessment of the evolved variants indicates that an increase in Cfr expression is accompanied by a decrease in fitness (**Fig. 2e**), start site selection in response to antibiotic pressure would mitigate detrimental impact on fitness while enabling higher resistance when acutely needed.

In addition to identifying mechanisms that increase Cfr-mediated resistance, directed evolution of Cfr also provided an indispensable reagent that enabled structural determination of the Cfr-modified ribosome. The high-resolution cryo-EM structure revealed that broad resistance is due to steric effects of the judiciously positioned methyl group within the shared binding site of PTC-targeting antibiotics. Lack of notable changes in position or orientation of A2503 or surrounding PTC nucleotides upon Cfr methylation suggests that the resulting modification does not obstruct the translation capabilities of the ribosome. This absence of PTC disruption is consistent with the observation that the fitness cost of Cfr acquisition is not due to ribosome modification, but rather results from expression of the exogenous protein (LaMarre et al., 2011). Importantly, overlay with existing structures containing PTC-targeting antibiotics provides direct visualization of chemical moieties that are sterically impacted by m^8A2503 and will inform design of antibiotic derivatives that can overcome resistance mediated by Cfr.

MATERIALS AND METHODS

E. coli strains and plasmids

E. coli ER2267 expressing Cfr from a pZA vector (Stojković et al., 2016; Wellner et al., 2013) was used in directed evolution experiments. Antibiotic resistance, fitness, *in vivo* RNA methylation, and protein/transcript expression, polysome analysis, and protein degradation experiments were conducted with *E. coli* BW25113 expressing Cfr protein from a pZA vector under the Ptet promoter (or Pcfr promoter where noted). *E. coli* BW25113 *acrB::kan*, where the efflux pump *acrB* was replaced with a kanamycin cassette, was used for antibiotic susceptibility testing of the oxazolidinone antibiotic, linezolid. For experiments for which tagless versions of evolved Cfr variants were used, comparisons were made to the *wildtype* Cfr protein to which the original C-terminal His tag had been removed. *E. coli* Rosetta2 BL21(DE3) pLysS was used for overexpression of N-His_6-SUMO-tagged Cfrs from a pET28a vector. *E. coli* MRE600 was used for preparation of Cfr-modified ribosomes for structural studies.

Cfr mutagenesis and selection scheme

The wild-type *cfr* gene (accession: EF450709.1) with a C-terminal His_6-tag, or pooled *cfr* genes from the previous round of evolution, were randomly mutagenized by error-prone polymerase chain reaction as described previously (Stojković et al., 2016). The mutagenized *cfr* gene pool was then recloned into a pZA vector and transformed into *E. coli* ER2267. The frequency of mutations was determined by sequencing randomly selected library variants and was on average 1-3 mutations per gene. *E. coli* transformants were then subjected to selection by plating cells on LB agar containing tiamulin (Wako Chemicals USA), in addition to 100 μg/mL ampicillin for plasmid maintenance and 20 ng/mL anhydrotetracycline (AHT, Sigma) for induction of Cfr expression. For each round of evolution, the *E. coli* transformants were divided equally and plated on 4-5 plates of LB agar containing different concentrations of tiamulin and grown at 37°C for up to 48 h. The tiamulin concentration was increased in 50-100 μg/ml increments. For example, in the first round of evolution the transformation was plated on the 150, 200, 250 and 300 μg/ml tiamulin plates, in the last round we selected on 250, 350, 450 and 550 μg/ml tiamulin plates. Two microliters were plated on tiamulin deficient plates in order to determine transformation efficiency. In general, colonies isolated from tiamulin plates in which the ≤10% of the transformants grew were taken for the next round. After 5 rounds of mutagenesis and selection, 2 rounds of enrichment (selection without mutagenesis) using high tiamulin concentrations (400-1500 μg/mL) was conducted. After each round of selection or enrichment, 5-10 randomly selected colonies were sequenced from each plate.

Determination of antibiotic resistance

Antibiotic resistance experiments by broth microdilution followed established protocols (Wiegand et al., 2008). In brief, 2 mL of LB media with selection antibiotic was inoculated with a freshly transformed colony containing either empty plasmid, CfrWT, or Cfr mutants. Cultures were grown at 37°C with shaking for approximately 2.5 h. After measuring the OD_{600} value, cultures were diluted to 10^6 cells and 50μL of this dilution was dispensed into 96-well plates containing 50 μL of LB media with antibiotic of

interest, ampicillin (100 µg/mL), and AHT (30 ng/mL). Antibiotic resistance of evolved Cfr variants were evaluated using 2-fold serial dilution of antibiotic with the following concentration ranges: tiamulin (50-6400 µg/mL, TCI America); clindamycin (50-6400 µg/mL, Cayman Chemical), chloramphenicol (0.5-64 µg/mL, Acros), linezolid (1-256 µg/mL, Acros), and trimethoprim (0.125 – 0.2 µg/mL, Sigma). Chloramphenicol resistance of single Cfr mutations were evaluated using concentrations of 1, 2-12 µg/mL (in 2 µg/mL-step increments), followed by 16-64 µg/mL (2-fold dilution). The minimum inhibitory concentration (MIC) required to inhibit visible bacterial growth was determined after incubating plates at 37°C with shaking for 18 h. Plate OD_{600} values were also recorded with a microtiter plate reader (SpectraMax M5, Molecular Devices). Antibiotic resistance determination on LB agar plates was conducted as described previously (Stojković et al., 2016; Wiegand et al., 2008). In brief, 3 µL of 10^8, 10^6, and 10^4 dilutions *E. coli* harboring Cfr were spotted on LB agar plates containing various concentrations of tiamulin. LB agar plates also contained ampicillin (100 µg/mL) and AHT (30 ng/mL). LB agar plates were incubated at 37°C for 24–48 h.

Oligo-protection of rRNA and MALDI-TOF analysis

E. coli expressing empty plasmid or Cfr were grown at 37°C to an OD_{600} of 0.4-0.6 with shaking by diluting an overnight culture 1:100 into LB media containing ampicillin (100 µg/mL) and AHT inducer (30 ng/mL). Total RNA purification, oligo-protection of the 23S rRNA fragment C2480-C2520, and RNaseT1 digestion was performed as described previously (Andersen et al., 2004; Stojković and Fujimori, 2015). Mass spectra were acquired in positive ion, reflectron mode on an AXIMA Performance MALDI TOF/TOF Mass Spectrometer (Shimadzu). Relative peak intensity values were calculated using the Shimadzu Biotech MALDI-MS software.

Expression and purification of Cfr

CfrWT and CfrV4 were expressed, purified, and reconstituted using modified published protocols (Stojković and Fujimori, 2015; Yan et al., 2010). In brief, N-His_6-SUMO-tagged CfrWT/V4 were overexpressed in minimal media conditions with 800 µM IPTG and 1,10-phenanthroline to obtain enzyme lacking a [4Fe-4S] iron-sulfur cluster. Minimal media also contained selection antibiotics kanamycin (50 µg/mL) and chloramphenicol (34 µg/mL). All purification steps were performed in a glovebox (MBraun, oxygen content below 1.8 ppm) that was cooled to 10°C. Cfr was purified by Talon chromatography (Clontech) from clarified lysates. Following chemical reconstitution of the [4Fe-4S], the N-His_6-SUMO-tag was cleaved by incubating the fusion protein with SenP1 protease (prepared in-house, 1 mg SenP1:100 mg Cfr) for 1 h at 10°C in buffer containing 50 mM EPPS (pH 8.5), 300 mM KCl 15% glycerol, and 5 mM DTT. The cleaved protein was purified away from SenP1 and the N-His_6-SUMO-tag by FPLC on a Mono Q 10/100 GL anion exchange column (GE Healthcare Life Sciences) using buffers containing 50 mM EPPS (pH 8.5), 50 mM or 1M KCl (low-salt or high-salt), 15% glycerol, and 5 mM DTT. Protein was eluted using a linear gradient of 100% low-salt to 100% high-salt buffer over 8 column volumes. Fractions containing apo-reconstituted, tag-less Cfr were combined, concentrated using a concentrator cell (Amicon Ultra- 0.5 mL, 30 MWCO), and stored at -80°C. Protein concentration was determined by Bradford assay (Bio-Rad).

Preparation of rRNA substrate

The *E. coli* 23S rRNA fragment 2447-2624 used for *in vitro* experiments was prepared using modified published protocols (Stojković and Fujimori, 2015). The desired DNA fragment was amplified from plasmid pKK3535 using previously established primers (Yan et al., 2010) and used as the template in the *in vitro* transcription reaction. Following DNase treatment and purification, RNA was precipitated overnight at −20°C by addition of 1/10th volume of 3 M NaOAc, pH 5.5 and 3 volumes of ethanol (EtOH). The RNA was then pelleted and washed with 70% aqueous EtOH, dried, and resuspended in nuclease-free water to obtain a final concentration of ~6 mg/mL. The rRNA fragment was refolded and purified by size exclusion chromatography. To refold the RNA, the sample was heated at 95°C for 2 min and then cooled to 65°C over 5 min. $MgCl_2$ was subsequently added to a final concentration of 10 mM prior to a final cooling step at room temperature for at least 30 min. After removing insoluble debris, RNA was purified by FPLC on a HiLoad 26/60 Superdex 200 column (GE Healthcare Life Sciences) using buffer containing 50 mM HEPES (pH 7.5), 10 mM $MgCl_2$, and 50 mM KCl. Fractions containing the desired rRNA product were combined and precipitated overnight at −20°C by addition of 1/10th volume of 3 M NaOAc, pH 5.5 and 3 volumes of EtOH. The RNA was then pelleted and washed with ice-cold 80% aqueous EtOH, dried, and resuspended in nuclease-free water. After confirming RNA purity on a denaturing 5% TBE, 7M Urea-PAGE gel, the RNA sample was concentrated to ~450 mM using a SpeedVac Vacuum Concentrator prior to storage at -80°C.

Cfr Kinetic Assay

Methylation activity of CfrWT and CfrV4 were assessed by monitoring radioactivity incorporation into RNA. Flavodoxin and flavodoxin reductase enzymes were prepared as described previously (McCusker et al., 2012). Prior to assembling reaction components, the RNA substrate was refolded as described above. Reactions were conducted in 52 µL volumes in an anaerobic chamber (MBraun, oxygen levels less than 1.8 ppm) under the following conditions: 100 mM HEPES (pH 8.0), 100 mM KCl, 10 mM $MgCl_2$, 2 mM DTT, 50 µM Flavodoxin, 25 µM Flavodoxin reductase, 100 µM rRNA substrate, 2 mM [^{3}H-methyl] *S*-adenosylmethionine (175.8 dpm/pmol), and 5 µM apo-reconstituted Cfr. Reactions were equilibrated at 37°C for 5 min and subsequently initiated by addition of NADPH (Sigma, final concentration 2 mM). The reaction was allowed to proceed at 37°C and timepoints at 0, 2, 4, 6, and 8 min of 10 µL volume were quenched by the addition of H_2SO_4 (50 mM final concentration). For each timepoint, the RNA volume was brought up to 100 µL with nuclease-free water and was purified away from other reaction components by an RNA Clean & Concentrator kit (Zymo Research) by following the manufacturer's instructions. Purified RNA eluate was added to Ultima Gold scintillation fluid, and the total amount of radioactivity incorporated in the product was detected using a Beckman–Coulter LS6500 scintillation counter. Amount of product generated at each time point was calculated by subtracting background radioactivity (t=0 min) and taking into account that 2 of the 3 tritium atoms from [^{3}H-methyl] *S*-adenosylmethionine would be incorporated into the final methylated RNA product (Bauerle et al., 2018; Yan and Fujimori, 2011).

Evaluation of Cfr protein expression by quantitative western blot

E. coli expressing empty plasmid, CfrWT, or Cfr mutants were grown at 37°C to an OD_{600} of ~0.4 with shaking by diluting an overnight culture 1:100 into 10 mL LB media containing ampicillin (100 µg/mL) and AHT inducer (30 ng/mL). Cells were harvested by centrifugation. Cell pellets were lysed for 15 min using B-PER Bacterial Protein Extraction Reagent (Thermo Scientific) containing DNase I (New England Biolabs) and 1X cOmplete, EDTA-free protease inhibitor cocktail (Roche). Whole cell lysate samples containing 4 µg of protein were fractionated using a 4–20% SDS-PAGE gel (Bio-Rad). Proteins were transferred to a 0.2 µm nitrocellulose membrane using a Trans-Blot Turbo transfer system (Bio-Rad) with a 7 min, mixed MW protocol. Membranes were incubated with TBST-Blotto buffer (50 mM Tris-pH 7.5, 150 mM NaCl, 0.1% Tween-20, 5% w/v Bio-Rad Blotting Grade Blocker) for 1 h at room temperature, followed by TBST-Blotto containing two primary antibodies: monoclonal mouse anti-FLAG M2 (1:2,000 dilution, Sigma) and monoclonal rabbit anti-RNA polymerase beta (1:2,000 dilution, Abcam) for 1 h at room temperature. After washing 3 x 5 min with TBST, membranes were then incubated overnight at 4°C with TBST-Blotto containing two secondary antibodies: goat anti-rabbit IgG cross-absorbed DyLight 680 (1:10,000 dilution, Thermo) and goat anti-mouse IgG cross-absorbed IRDye 800CW (1:10,000 dilution, Abcam). Membranes were rinsed 3 x 5 min with TBST and allowed to dry completely prior imaging using a Bio-Rad ChemiDoc Molecular Imager. Quantification was performed using Image Lab Software (Bio-Rad) within the linear range of detection. The house-keeping protein RNA polymerase beta, which was stably expressed in all experimental conditions, was used as an internal loading control.

Determination of *E. coli* growth rate

E. coli expressing empty plasmid, CfrWT, or Cfr variants were grown at 37°C with shaking by diluting an 50 µL of an overnight culture into 10 mL of LB media containing ampicillin (100 µg/mL) and AHT inducer (30 ng/mL). OD_{600} values were recorded every 20 min with a microtiter plate reader (SpectraMax M5, Molecular Devices).

qPCR Primer Design and Validation

qPCR primer sequences for *cfr, recA,* and *luc* were designed using NCBI Primer Blast. Template accession numbers, amplicon length, and primer sequences are described in **Supplementary Table 1**. Primer sequences for *rrsA* were used as published previously (Zhou et al., 2011). For each primer pair primer, qPCR was performed on a 10-fold dilution series of desired samples. Amplification efficiency was calculated from the slope of the graph of Cq values plotted against $\log_{10}$ of the at least four template concentrations. Primers for recA: $Y = -3.238*X + 38.46$, $R^2 = 0.9992$, PCR efficiency = 103.6%. Primers for luc: $Y = -3.316*X + 34.52$, $R^2 = 0.9967$, PCR efficiency = 100.2%. Primers for cfr: $Y = -3.254*X + 37.52$, $R^2 = 0.9960$, PCR efficiency = 102.9%. Primers for rrsA: $Y = -3.629*X + 32.24$, $R^2 = 0.9965$, PCR efficiency = 90.0%.

Determination of Cfr mRNA expression by RT-qPCR

Bacterial growth. *E. coli* expressing empty plasmid control, CfrWT, or Cfr variants were grown at 37°C with shaking by diluting an overnight culture 1:100 into 5 mL of LB media containing ampicillin (100 µg/mL) and AHT inducer (30 ng/mL). When cells reached an OD_{600} of ~ 0.4, RNAprotect Bacteria

Reagent (Qiagen) was added to the culture following manufacturer's instructions. Cells were then harvested by centrifugation for 10 min at 5000 x *g* at 4°C and frozen on dry ice.

Total RNA isolation and DNase treatment. Pellets were then thawed and resuspended in 200 µL of lysis buffer containing 30 mM Tris-HCl (pH 8.0), 0.1 mM EDTA, 15 mg/mL lysozyme, and Proteinase K (New England Biolabs). Following lysis for 10 min at room temperature, total RNA was isolated using a RNeasy mini kit (QIAGEN) following the manufacturer's instructions. Yield and purity of isolated RNA was assessed by NanoDrop UV spectrophotometer (Thermo). RNA integrity was assessed by performing 1% TBE agarose gel electrophoresis with samples that had been boiled for 95°C for 5 min in RNA loading dye (New England Biolabs). Genomic DNA was eliminated by incubating 2 µg of RNA with 2 U of RQ1 RNase-free DNase I (Promega) for 30 min at 30°C. The DNase reaction was halted by the addition of RQ1 Stop Solution (Promega) and incubation for 10 min at 65° C.

cDNA synthesis. Reverse transcription was performed using the iScript cDNA Synthesis Kit (Bio-Rad) following the manufacturer's instructions with 10-fold diluted DNase-treated RNA. In brief, reactions of 20 µL volume were prepared by combining 4 µL 5X iScript buffer, 1 µL iScript RNase H+ MMLV reverse transcriptase, 11 µL nuclease-free water, and 4 µL of RNA. Reactions were incubated for 5 min at 25 °C, followed by 20 min at 42 °C and 1 min at 95 °C. If not used immediately, cDNA was stored at -20°C.

RT-qPCR. SsoAdvanced Universal SYBR Green Supermix (Bio-Rad) was used for 10 µL qPCR reactions. Each reaction contained 5 µL of 2X Supermix, 0.3 µM of each forward and reverse primer, and 4 µL of diluted cDNA. The cDNA was diluted 40-fold for reactions with *cfr* primers and 4,000-fold for reactions *rrsA* primers. Reactions were prepared in a 96-well PCR Plate (Bio-Rad, MLL9601) and run on a Bio-Rad CFX qPCR Machine. The thermal cycling conditions were as follows: 98°C for 30 s, followed by 35 cycles of 98°C for 10 s and 60°C for 45 s with plate read, ending with melt curve analysis using 5s, 0.5 °C increment steps from 65 °C to 95 °C. A no template control and no reverse transcription control were included on each plate for each primer pair. Cq values were determined using CFX Maestro Software using a single threshold method. For each sample, the average of three triplicate Cq values was used for further analysis. Relative transcript expression was calculated using the Pfaffl method (Pfaffl, 2001). Expression was normalized to *rrsA* transcripts which is stably expressed in *E. coli* BW25113 (Zhou et al., 2011) and across our experimental conditions.

Polysome analysis

Lysate preparation and sucrose gradient fractionation were adapted from previously published protocols with modification (Li et al., 2014; Mohammad and Buskirk, 2019).

Lysate preparation. *E. coli* expressing empty plasmid control, CfrWT, or Cfr mutants were grown at 37°C with shaking by diluting an overnight culture 1:100 into 400 mL of LB media containing ampicillin (100 µg/mL) and AHT inducer (30 ng/mL). Cells were harvested at an OD_{600} ~0.4-0.5 in 200 mL batches by rapid filtration at 37°C followed by flash freezing in liquid nitrogen as described previously(Li et al., 2014). Each frozen cell pellet was combined with 650 µL lysis buffer as frozen droplets containing 20 mM Tris (pH 8.0), 10 mM $MgCl_2$, 100 mM NH_4Cl, 5 mM $CaCl_2$, 0.4% Triton X-100, 0.1% NP-40, 100 U/ml RNase-free DNase I (Roche), and 10 U/mL SUPERase-In (Invitrogen). Cells with lysis buffer were pulverized in a 10 mL jar containing a 12 mm grinding ball using a

TissueLyser II (QIAGEN) by performing 5 rounds of 3 min at 15 Hz. Canisters were pre-chilled by submersion in liquid nitrogen for at least 1 min prior to each round of pulverization. Lysates were recovered from the frozen jars using a spatula pre-chilled in liquid nitrogen and stored at -80ºC until further use.

Sucrose Gradient Fractionation. Pulverized lysates were thawed at 30ºC for 2 min followed by an ice-water bath for 20 min. Lysates were clarified by centrifugation at 20,000 x *g* for 10 min at 4ºC. The RNA concentration of the clarified lysate was measured by NanoDrop UV spectrophotometer (Thermo) and diluted to 2.5 mg/mL with lysis buffer. Ribosome and mRNA components were separated on a linear, 12 mL, 10-55% (w/v) sucrose gradient containing 20 mM Tris (pH 8.0), 10 mM $MgCl_2$, 100 mM NH_4Cl, 2 mM DTT, and 10 U/mL SUPERase-In. Sucrose gradients were generated using a Bio-Comp Gradient Master with the following program: Time = 1:58 s; Angle = 81.5º, Speed = 16 rpm. For each biological sample, 190 µL (~0.5 mg RNA) of clarified lysate was loaded onto sucrose gradients in duplicate. Ultracentrifugation was performed using a SW Ti41 rotor (Beckman Coulter) for 201,000 x *g* for 2.5 h at 4ºC. Gradients were fractionated using a Bio-Comp Fractionator in 20 fractions at a speed of 0.25 mm/sec where absorbance at 260 nm was continuously monitored.

RNA Extraction and DNase Treatment. Fractions 1+2, 3+4, 16+17, and 18+19 were combined. RNA was extracted from uniform volumes of each fraction or combination of fractions. RNA extraction was performed by adding one volume of TRIzol reagent (Invitrogen), mixing until homogeneous, and incubating at room temperature for 5 min. Samples were then incubated at room temperature for another 5 min following the addition of 0.4 volumes of chloroform. After centrifugation for 15 min at 12,000 x *g* at 4ºC, the aqueous supernatant was transferred to a new tube to which 250 pg of a luciferase control RNA spike-in (luc, Promega). RNA was precipitated overnight at -20ºC by the addition of 1 volume of isopropanol and 2 µL of GlycoBlue (15 mg/mL, Invitrogen). RNA was pelleted by centrifugation, washed twice with 75% ice-cold, aqueous ethanol, and allowed to dry at room temperature for ~30 min. The RNA was then resuspended in 20 µL of nuclease-free water. RNA quality and concentration were assessed by a NanoDrop UV spectrophotometer (Thermo). Genomic DNA was eliminated by incubating 10 µL of isolated RNA with 1 U of RQ1 RNase-free DNase I (Promega) for 30 min at 30°C. The DNase reaction was halted by the addition of RQ1 Stop Solution (Promega) and incubation for 10 min at 65°C.

cDNA synthesis and RT-qPCR. Reverse transcription was performed using the iScript cDNA Synthesis Kit (Bio-Rad) following the manufacturer's instructions. In brief, reactions of 20 µL volume were prepared by combining 4 µL 5X iScript buffer, 1 µL iScript RNase H+ MMLV reverse transcriptase, 5 µL nuclease-free water, and 10 µL of DNase-treated RNA. Reactions were incubated for 5 min at 25 °C, followed by 20 min at 42 °C and 1 min at 95 °C. SsoAdvanced Universal SYBR Green Supermix (Bio-Rad) was used for 10 µl qPCR reactions in a 96-well plate as described above. Each reaction contained 5 µL of 2X Supermix, 0.3 µM of each forward and reverse primer, and 4 µL of 10-fold diluted cDNA. Reactions containing cfr, recA, and luc primers (**Supplementary Table 1**) were performed for each fraction, including a no template control and no reverse transcription control for each primer set on each plate. The average of three triplicate Cq values was used for further analysis.

Data Analysis. Normalized mRNA distribution profiles for the target mRNAs were calculated as described previously (Pringle et al., 2019). In brief, the relative abundance of each target mRNA

normalized to luciferase RNA spike-in. The percentage of target mRNA found across gradient fractions was calculated by dividing the amount of target mRNA detected in one fraction by the sum of the target mRNA detected in all fractions.

Protein Degradation Assay

Bacterial growth and rifampicin treatment. *E. coli* expressing CfrWT or Cfr mutants were grown at 37ºC with shaking by diluting an overnight culture 1:100 into 25 mL of LB media containing ampicillin (100 µg/mL) and AHT inducer (30 ng/mL). When cells reached an OD_{600} ~0.4-0.5, rifampicin (Sigma) was subsequently added to a final concentration of 100 µg/mL, and cultures were allowed continued incubation at 37ºC with shaking. Timepoints at 0, 20, 40, 60, 80, 100 min were harvested by centrifuging 3 mL of the culture at 8,000 rpm at 4ºC for 10 min, decanting the supernatant, and immediately flash-freezing the pellet in liquid nitrogen. Cell pellets for each time point were lysed using B-PER Bacterial Protein Extraction Reagent as described above.

Western blot. Whole cell lysate samples containing 5 µg of protein were fractionated on a 4-20% SDS-PAGE gel and transferred onto a 0.2 µm nitrocellulose membrane as described above. Membranes were stained with Ponceau S stain (0.1% w/v Ponceau S, 5% v/v acetic acid) and imaged using a Bio-Rad ChemiDoc Molecular Imager. After blocking in TBST-Blotto buffer for 1 h at room temperature, membranes were incubated with TBST-Blotto containing primary monoclonal mouse anti-FLAG M2 antibody (1:2,000 dilution, Sigma) or monoclonal mouse anti-GAPDH antibody (1:2,000 dilution, Abcam) for 1 h at room temperature. After washing 3 x 5 min with TBST, membranes were incubated overnight at 4ºC with TBST-Blotto containing a secondary antibody, goat anti-mouse cross-absorbed IRDye 800CW (1:10,000 dilution, Abcam). Membranes were rinsed and imaged as described above.

Data Analysis. Quantification was performed using Image Lab Software (Bio-Rad) within the linear range of detection. The Ponceau S total protein stain was used to normalize for differential sample loading. Percentage (%) of initial Cfr protein remaining was calculated by dividing the amount of Cfr protein at a given time point after rifampicin treatment by the amount of Cfr protein prior to rifampicin treatment (t = 0 min).

Purification of Cfr-modified *E. coli* ribosome

Cfr-modified, 70S ribosomal subunit was purified from *E. coli* MRE600 expressing CfrV7 variant using previously published protocol with modification (Mehta et al., 2012; Stojković et al., 2020). In short, *E. coli* transformed with pZA-encoded CfrV7 were grown to an OD_{600} of 0.5 in LB media containing ampicillin (100 µg/mL) and AHT inducer (30 ng/mL) at 37°C with shaking. Cells were harvested by centrifugation, washed, and lysed by using a microfluidizer. The lysate was clarified by ultracentrifugation at 30,000 x *g* 30 min at 4ºC using a Ti45 rotor (Beckman Coulter) twice. The recovered supernatant was applied to a 32 % w/v sucrose cushion in buffer containing 20 mM Hepes-KOH (pH 7.5), 500 mM NH_4Cl, 20 mM $Mg(OAc)_2$, 0.5 mM EDTA, 6 mM β-mercaptoethanol, 10 U/mL SuperASE-In and was ultracentrifuged at 100,000 x *g* for for 16 h at 4 ˚C in a SW Ti41 rotor (Beckman Coulter). After removing the supernatant, the pellet was resuspended slowly at 4ºC over 1 h in Buffer A containing 20 mM Hepes-KOH (pH 7.5), 200 mM NH_4Cl, 20 mM $Mg(OAc)_2$, 0.1 mM

EDTA, 6 mM β-mercaptoethanol, 10 U/mL SuperASE-In. Particulates that were not resuspended were removed by centrifugation at 10,000 rpm for 10 min at 4°C. Sample concentration was determined by NanoDrop UV spectrophotometer (Thermo), where A_{260}=1 corresponds to 24 pmol of 70S ribosome. Tight-coupled 70S ribosomes were purified as described previously (Khusainov et al., 2017). In brief, 70S ribosomes were purified on a 15-30% w/v sucrose gradient in Buffer A. Sucrose gradients were generated using a Bio-Comp Gradient Master. 300-400 pmol of 70S ribosomes were loaded on each sucrose gradient. Ultracentrifugation was performed using a SW Ti41 rotor (Beckman Coulter) for 75,416 x *g* for 16 h at 4ºC. Gradients were fractionated using a Bio-Comp Fractionator in 20 fractions at a speed of 0.25 mm/sec where absorbance at 260 nm was continuously monitored. Fractions corresponding to 70S ribosomes were combined and precipitated by slow addition at 4ºC of PEG 20,000 in Buffer A to a final concentration of 9% w/v. Ribosomes were isolated by centrifugation for 10 min at 17,500 x *g*. After removing the supernatant, ribosomes were slowly resuspended overnight at 4ºC in buffer containing 50 mM Hepes-KOH (pH 7.5), 150 mM KOAc, 20 mM $Mg(OAc)_2$, 7 mM β-mercaptoethanol, 20 U/mL SuperASE-In.

Cryo-EM analysis

Purified 70S ribosomal subunits were diluted from 2 to 0.5 mg/ml in Buffer A, applied to 300-mesh carbon coated (2nm thickness) holey carbon Quantifoil 2/2 grids (Quantifoil Micro Tools) and flash-frozen as described in (Khatter et al., 2015). Data were collected using serialEM on the in-house Titan Krios X-FEG instrument (Thermo Fisher Scientific) operating at an acceleration voltage of 300 kV and a nominal underfocus of Δz = 0.2 to 1.5 µm at a nominal magnification of 29 000 (calibrated physical pixel size of 0.822 Å). We recorded 2055 movies using a K2 direct electron detector camera in super-resolution mode with dose fractionation (80 individual frames were collected, starting from the first one). Total exposure time was 8 s, with the total dose of 80 e- (or 1 e-/Å2/frame). Images in the stack were aligned using the whole-image motion correction and patch motion correction (5 × 5 patches) methods in MotionCor2 (Zheng et al., 2017). Before image processing, all micrographs were checked for quality and 1531 best were selected for the next step of image processing. The contrast transfer function of each image was determined using GCTF (Zhang, 2016) as a standalone program. For particle selection we have used Relion 3.0 autopicking procedure (Scheres, 2012). For the first steps of image processing we used data binned by a factor of 8 (C8 images). During the first round of 2D classification we removed only images with ice or other contaminants. Subsequently, the initial structure was generated using the *ab initio* procedure in CryoSPARC v2.0. Following this step, we performed Relion 3D classification with bin by four data (C4) in order to exclude bad particles. The resulting 141 549 particle images of ribosomes were used for subsequent classification and refinement procedures. For the initial refinement we used a spherical mask, which was followed by further refinement using a mask around the stable part of 50S (excluding L1 stalk, L7/L12 region). A further improved cryo-EM map was obtained by using CTF-refinement procedure from Relion 3.0. The post-processing procedure implemented in Relion 3.0 (Scheres, 2012) was applied to the final maps with appropriate masking, B-factor sharpening (automatic *B*-factor estimation was -55.86) and resolution estimation to avoid over-fitting (final resolution after post-processing with 50S mask applied was 2.7 Å). Subsequently the stack of CTF-refined particles was processed in a new version of CryoSPARC v2.0 (Punjani et al.,

2017). After homogeneous refinement the same stack of particles was additionally refined in cisTEM (Grant et al., 2018). After Auto-Refine (with automasking within cisTEM) we performed local refinement using 50S mask (the same one used for refinement in Relion) and also applied per particle CTF refinement as implemented in cisTEM software. After such refinement the resolution was improved to 2.2 Å (**Extended Data Fig. 6**). This map after Sharpen3D (Grant et al., 2018) was used for model building and map interpretation.

Atomic model building and refinement

The final model of the 50S subunit was generated by multiple rounds of model building in Coot (Emsley et al., 2010) and subsequent refinement in PHENIX (Adams et al., 2010). The restraints for the novel m^2m^8A nucleotide for the atomic model fitting and refinements were generated using eLBOW (Moriarty et al., 2009). The atomic model of the 50S subunit from the *E. coli* ribosome structure (PDB 6PJ6) (Stojković et al., 2020) was used as a starting point and refined against the experimental cryo-EM map by iterative manual model building and restrained parameter-refinement protocol (real-space refinement, positional refinement, and simulated annealing). Final atomic model comprised of ~92 736 atoms (excluding hydrogens) across the 3015 nucleotides and 3222 amino acids of 28 ribosomal proteins. Proteins L7, L10, L11 and L31 were not modelled in. In addition, 179 Mg^{2+}, 2716 water molecules, one Zn^{2+} and one Na^{+} were included in the final model. Prior to running MolProbity (Chen et al., 2010) analysis, nucleotides 878–898, 1052–1110, 2101–2189 of 23S rRNA, and ribosomal protein L9 were removed, due to their high degree of disorder. Overall, protein residues and nucleotides show well-refined geometrical parameters (**Supplementary Table 6**). Figures were prepared using Pymol Molecular Graphics System, Version 2.4.1 unless otherwise noted.

qPTxM analysis of post-transcriptional modifications

The final model and map were run through qPTxM (Stojković et al., 2020) with default parameters except for d_min=2 and cc_threshold=0.5 to search for evidence of posttranscriptional modifications. Of a total of 39 sites with density suggesting possible modifications, two were C8-methyl adenosines, A556 and A2503. None of the identified sites were 2'O-methyl cytosines. To calculate expected density dropoff curves for methylated and unmethylated nucleotides, the *phenix.fmodel* (Adams et al., 2010) tool was used to generate noise-free maps from models of a single nucleotide in each state, and scripts modified from qPTxM were used to collect measurements of the density at 0.1 Å intervals along the vector of the proposed methylation. Means and standard deviations were calculated for densities at the four positions tested by qPTxM on each nucleotide, from which Z-scores were then calculated for selected nucleotides. To measure densities for both the best tested rotamer of m(2'O)C 2498 and the modeled rotamer, densities along the 2'O-methyl bond were compared between the files generated by qPTxM run twice as described above, once with prune=True (removing the modeled methyl group and placing the rotameric methyl with the strongest density) and once with prune=False (leaving the modeled methyl group intact).

REFERENCES

Adams PD, Afonine PV, Bunkóczi G, Chen VB, Davis IW, Echols N, Headd JJ, Hung L-W, Kapral GJ, Grosse-Kunstleve RW, McCoy AJ, Moriarty NW, Oeffner R, Read RJ, Richardson DC, Richardson JS, Terwilliger TC, Zwart PH. 2010. PHENIX: a comprehensive Python-based system for macromolecular structure solution. *Acta Crystallogr D Biol Crystallogr* **66**:213–221.

Andersen TE, Porse BT, Kirpekar F. 2004. A novel partial modification at C2501 in Escherichia coli 23S ribosomal RNA. *RNA* **10**:907–913.

Arenz S, Wilson DN. 2016. Blast from the Past: Reassessing Forgotten Translation Inhibitors, Antibiotic Selectivity, and Resistance Mechanisms to Aid Drug Development. *Mol Cell* **61**:3–14.

Arias CA, Vallejo M, Reyes J, Panesso D, Moreno J, Castañeda E, Villegas MV, Murray BE, Quinn JP. 2008. Clinical and microbiological aspects of linezolid resistance mediated by the cfr gene encoding a 23S rRNA methyltransferase. *J Clin Microbiol* **46**:892–896.

Barlow M, Hall BG. 2003. Experimental prediction of the natural evolution of antibiotic resistance. *Genetics* **163**:1237–1241.

Bauerle MR, Grove TL, Booker SJ. 2018. Investigation of Solvent Hydron Exchange in the Reaction Catalyzed by the Antibiotic Resistance Protein Cfr. *Biochemistry* **57**:4431–4439.

Bentele K, Saffert P, Rauscher R, Ignatova Z, Blüthgen N. 2013. Efficient translation initiation dictates codon usage at gene start. *Mol Syst Biol* **9**:675.

Besier S, Ludwig A, Zander J, Brade V, Wichelhaus TA. 2008. Linezolid resistance in Staphylococcus aureus: gene dosage effect, stability, fitness costs, and cross-resistances. *Antimicrob Agents Chemother* **52**:1570–1572.

Bhattacharyya S, Jacobs WM, Adkar BV, Yan J, Zhang W, Shakhnovich EI. 2018. Accessibility of the Shine-Dalgarno Sequence Dictates N-Terminal Codon Bias in E. coli. *Mol Cell* **70**:894–905.e5.

Boël G, Letso R, Neely H, Price WN, Wong K-H, Su M, Luff J, Valecha M, Everett JK, Acton TB, Xiao R, Montelione GT, Aalberts DP, Hunt JF. 2016. Codon influence on protein expression in E. coli correlates with mRNA levels. *Nature* **529**:358–363.

Bonilla H, Huband MD, Seidel J, Schmidt H, Lescoe M, McCurdy SP, Lemmon MM, Brennan LA, Tait-Kamradt A, Puzniak L, Quinn JP. 2010. Multicity outbreak of linezolid-resistant Staphylococcus epidermidis associated with clonal spread of a cfr-containing strain. *Clin Infect Dis* **51**:796–800.

Brock JE, Paz RL, Cottle P, Janssen GR. 2007. Naturally occurring adenines within mRNA coding sequences affect ribosome binding and expression in Escherichia coli. *J Bacteriol* **189**:501–510.

Cai JC, Hu YY, Zhou HW, Chen G-X, Zhang R. 2015. Dissemination of the same cfr-carrying plasmid among methicillin-resistant Staphylococcus aureus and coagulase-negative staphylococcal isolates in China. *Antimicrob Agents Chemother* **59**:3669–3671.

Cambray G, Guimaraes JC, Arkin AP. 2018. Evaluation of 244,000 synthetic sequences reveals design principles to optimize translation in Escherichia coli. *Nat Biotechnol* **36**:1005–1015.

Chen VB, Arendall WB 3rd, Headd JJ, Keedy DA, Immormino RM, Kapral GJ, Murray LW, Richardson JS, Richardson DC. 2010. MolProbity: all-atom structure validation for macromolecular crystallography. *Acta Crystallogr D Biol Crystallogr* **66**:12–21.

Del Tito BJ Jr, Ward JM, Hodgson J, Gershater CJ, Edwards H, Wysocki LA, Watson FA, Sathe G, Kane JF. 1995. Effects of a minor isoleucyl tRNA on heterologous protein translation in Escherichia coli. *J Bacteriol* **177**:7086–7091.

Dong H, Nilsson L, Kurland CG. 1996. Co-variation of tRNA Abundance and Codon Usage inEscherichia coliat Different Growth Rates. *Journal of Molecular Biology*.

doi:10.1006/jmbi.1996.0428
Dortet L, Glaser P, Kassis-Chikhani N, Girlich D, Ichai P, Boudon M, Samuel D, Creton E, Imanci D, Bonnin R, Fortineau N, Naas T. 2018. Long-lasting successful dissemination of resistance to oxazolidinones in MDR Staphylococcus epidermidis clinical isolates in a tertiary care hospital in France. *J Antimicrob Chemother* **73**:41–51.
Ebihara N, Hitomi S, Goto M, Koganemaru H, Sekiguchi Y. 2014. Recovery of linezolid-resistant, methicillin-susceptible Staphylococcus aureus in a case of implanted pacemaker-associated infection. *JMM Case Reports* **1**:e001297.
Emsley P, Lohkamp B, Scott WG, Cowtan K. 2010. Features and development ofCoot. *Acta Crystallographica Section D Biological Crystallography*. doi:10.1107/s0907444910007493
Farney EP, Feng SS, Schäfers F, Reisman SE. 2018. Total Synthesis of (+)-Pleuromutilin. *J Am Chem Soc* **140**:1267–1270.
Giessing AMB, Jensen SS, Rasmussen A, Hansen LH, Gondela A, Long K, Vester B, Kirpekar F. 2009. Identification of 8-methyladenosine as the modification catalyzed by the radical SAM methyltransferase Cfr that confers antibiotic resistance in bacteria. *RNA* **15**:327–336.
Goethe O, Heuer A, Ma X, Wang Z, Herzon SB. 2019. Antibacterial properties and clinical potential of pleuromutilins. *Nat Prod Rep* **36**:220–247.
Goodman DB, Church GM, Kosuri S. 2013. Causes and Effects of N-Terminal Codon Bias in Bacterial Genes. *Science*. doi:10.1126/science.1241934
Gorochowski TE, Ignatova Z, Bovenberg RAL, Roubos JA. 2015. Trade-offs between tRNA abundance and mRNA secondary structure support smoothing of translation elongation rate. *Nucleic Acids Res* **43**:3022–3032.
Gottesman S. 2003. Proteolysis in bacterial regulatory circuits. *Annu Rev Cell Dev Biol* **19**:565–587.
Grant T, Rohou A, Grigorieff N. 2018. cisTEM, user-friendly software for single-particle image processing. *eLife*. doi:10.7554/elife.35383
Grove TL, Benner JS, Radle MI, Ahlum JH. 2011a. A radically different mechanism for S-adenosylmethionine–dependent methyltransferases.
Grove TL, Benner JS, Radle MI, Ahlum JH, Landgraf BJ, Krebs C, Booker SJ. 2011b. A Radically Different Mechanism for S-Adenosylmethionine-Dependent Methyltransferases. *Science*. doi:10.1126/science.1200877
Kaminska KH, Purta E, Hansen LH, Bujnicki JM, Vester B, Long KS. 2010. Insights into the structure, function and evolution of the radical-SAM 23S rRNA methyltransferase Cfr that confers antibiotic resistance in bacteria. *Nucleic Acids Res* **38**:1652–1663.
Kehrenberg C, Aarestrup FM, Schwarz S. 2007. IS21-558 insertion sequences are involved in the mobility of the multiresistance gene cfr. *Antimicrob Agents Chemother* **51**:483–487.
Kehrenberg C, Schwarz S, Jacobsen L, Hansen LH, Vester B. 2005. A new mechanism for chloramphenicol, florfenicol and clindamycin resistance: methylation of 23S ribosomal RNA at A2503. *Mol Microbiol* **57**:1064–1073.
Khatter H, Myasnikov AG, Natchiar SK, Klaholz BP. 2015. Structure of the human 80S ribosome. *Nature* **520**:640–645.
Khusainov I, Vicens Q, Bochler A, Grosse F, Myasnikov A, Ménétret J-F, Chicher J, Marzi S, Romby P, Yusupova G, Yusupov M, Hashem Y. 2017. Structure of the 70S ribosome from human pathogen Staphylococcus aureus. *Nucleic Acids Res* **45**:1026.
Kudla G, Murray AW, Tollervey D, Plotkin JB. 2009. Coding-sequence determinants of gene expression in Escherichia coli. *Science* **324**:255–258.
LaMarre J, Mendes RE, Szal T, Schwarz S, Jones RN, Mankin AS. 2013. The genetic environment of

the cfr gene and the presence of other mechanisms account for the very high linezolid resistance of Staphylococcus epidermidis isolate 426-3147L. *Antimicrob Agents Chemother* **57**:1173–1179.

LaMarre JM, Locke JB, Shaw KJ, Mankin AS. 2011. Low fitness cost of the multidrug resistance gene cfr. *Antimicrob Agents Chemother* **55**:3714–3719.

Layer F, Vourli S, Karavasilis V, Strommenger B, Dafopoulou K, Tsakris A, Werner G, Pournaras S. 2018. Dissemination of linezolid-dependent, linezolid-resistant Staphylococcus epidermidis clinical isolates belonging to CC5 in German hospitals. *J Antimicrob Chemother* **73**:1181–1184.

Lazaris A, Coleman DC, Kearns AM, Pichon B, Kinnevey PM, Earls MR, Boyle B, O'Connell B, Brennan GI, Shore AC. 2017. Novel multiresistance cfr plasmids in linezolid-resistant methicillin-resistant Staphylococcus epidermidis and vancomycin-resistant Enterococcus faecium (VRE) from a hospital outbreak: co-location of cfr and optrA in VRE. *J Antimicrob Chemother* **72**:3252–3257.

Li G-W, Burkhardt D, Gross C, Weissman JS. 2014. Quantifying Absolute Protein Synthesis Rates Reveals Principles Underlying Allocation of Cellular Resources. *Cell*. doi:10.1016/j.cell.2014.02.033

Lobritz M, Hutton-Thomas R, Marshall S, Rice LB. 2003. Recombination proficiency influences frequency and locus of mutational resistance to linezolid in Enterococcus faecalis. *Antimicrob Agents Chemother* **47**:3318–3320.

Locke JB, Morales G, Hilgers M, G C K, Rahawi S, José Picazo J, Shaw KJ, Stein JL. 2010. Elevated linezolid resistance in clinical cfr-positive Staphylococcus aureus isolates is associated with co-occurring mutations in ribosomal protein L3. *Antimicrob Agents Chemother* **54**:5352–5355.

Long KS, Poehlsgaard J, Kehrenberg C, Schwarz S, Vester B. 2006. The Cfr rRNA methyltransferase confers resistance to Phenicols, Lincosamides, Oxazolidinones, Pleuromutilins, and Streptogramin A antibiotics. *Antimicrob Agents Chemother* **50**:2500–2505.

Looman AC, Bodlaender J, Comstock LJ, Eaton D, Jhurani P, de Boer HA, van Knippenberg PH. 1987. Influence of the codon following the AUG initiation codon on the expression of a modified lacZ gene in Escherichia coli. *EMBO J* **6**:2489–2492.

McCusker KP, Medzihradszky KF, Shiver AL, Nichols RJ, Yan F, Maltby DA, Gross CA, Fujimori DG. 2012. Covalent intermediate in the catalytic mechanism of the radical S-adenosyl-L-methionine methyl synthase RlmN trapped by mutagenesis. *J Am Chem Soc* **134**:18074–18081.

Mehta P, Woo P, Venkataraman K, Karzai AW. 2012. Ribosome Purification Approaches for Studying Interactions of Regulatory Proteins and RNAs with the Ribosome In: Keiler KC, editor. Bacterial Regulatory RNA: Methods and Protocols. Totowa, NJ: Humana Press. pp. 273–289.

Mohammad F, Buskirk AR. 2019. Protocol for Ribosome Profiling in Bacteria. *Bio Protoc* **9**. doi:10.21769/BioProtoc.3468

Morales G, Picazo JJ, Baos E, Candel FJ, Arribi A, Peláez B, Andrade R, de la Torre M-A, Fereres J, Sánchez-García M. 2010. Resistance to linezolid is mediated by the cfr gene in the first report of an outbreak of linezolid-resistant Staphylococcus aureus. *Clin Infect Dis* **50**:821–825.

Moriarty NW, Grosse-Kunstleve RW, Adams PD. 2009. electronic Ligand Builder and Optimization Workbench (eLBOW): a tool for ligand coordinate and restraint generation. *Acta Crystallogr D Biol Crystallogr* **65**:1074–1080.

Murphy SK, Zeng M, Herzon SB. 2017. A modular and enantioselective synthesis of the pleuromutilin antibiotics. *Science* **356**:956–959.

Nakamura Y, Gojobori T, Ikemura T. 2000. Codon usage tabulated from international DNA sequence databases: status for the year 2000. *Nucleic Acids Res* **28**:292.

Pfaffl MW. 2001. A new mathematical model for relative quantification in real-time RT-PCR. *Nucleic*

Acids Res **29**:e45.
Polikanov YS, Starosta AL, Juette MF, Altman RB, Terry DS, Lu W, Burnett BJ, Dinos G, Reynolds KA, Blanchard SC, Steitz TA, Wilson DN. 2015. Distinct tRNA Accommodation Intermediates Observed on the Ribosome with the Antibiotics Hygromycin A and A201A. *Mol Cell* **58**:832–844.
Pringle ES, McCormick C, Cheng Z. 2019. Polysome Profiling Analysis of mRNA and Associated Proteins Engaged in Translation. *Curr Protoc Mol Biol* **125**:e79.
Punjani A, Rubinstein JL, Fleet DJ, Brubaker MA. 2017. cryoSPARC: algorithms for rapid unsupervised cryo-EM structure determination. *Nat Methods* **14**:290–296.
Purta E, O'Connor M, Bujnicki JM, Douthwaite S. 2009. YgdE is the 2′-O-ribose methyltransferase RlmM specific for nucleotide C2498 in bacterial 23S rRNA. *Mol Microbiol* **72**:1147–1158.
Riba A, Di Nanni N, Mittal N, Arhné E, Schmidt A, Zavolan M. 2019. Protein synthesis rates and ribosome occupancies reveal determinants of translation elongation rates. *Proc Natl Acad Sci U S A* **116**:15023–15032.
Sato T, Terabe M, Watanabe H, Gojobori T, Hori-Takemoto C, Miura Ki. 2001. Codon and base biases after the initiation codon of the open reading frames in the Escherichia coli genome and their influence on the translation efficiency. *J Biochem* **129**:851–860.
Scheres SHW. 2012. RELION: implementation of a Bayesian approach to cryo-EM structure determination. *J Struct Biol* **180**:519–530.
Schlünzen F, Zarivach R, Harms J, Bashan A, Tocilj A, Albrecht R, Yonath A, Franceschi F. 2001. Structural basis for the interaction of antibiotics with the peptidyl transferase centre in eubacteria. *Nature* **413**:814–821.
Schwarz S, Shen J, Kadlec K, Wang Y, Brenner Michael G, Feßler AT, Vester B. 2016. Lincosamides, Streptogramins, Phenicols, and Pleuromutilins: Mode of Action and Mechanisms of Resistance. *Cold Spring Harb Perspect Med* **6**. doi:10.1101/cshperspect.a027037
Schwarz S, Werckenthin C, Kehrenberg C. 2000. Identification of a Plasmid-Borne Chloramphenicol-Florfenicol Resistance Gene inStaphylococcus sciuri. *Antimicrob Agents Chemother* **44**:2530–2533.
Shen J, Wang Y, Schwarz S. 2013. Presence and dissemination of the multiresistance gene cfr in Gram-positive and Gram-negative bacteria. *J Antimicrob Chemother* **68**:1697–1706.
Smith LK, Mankin AS. 2008. Transcriptional and translational control of the mlr operon, which confers resistance to seven classes of protein synthesis inhibitors. *Antimicrob Agents Chemother* **52**:1703–1712.
Stenström CM, Holmgren E, Isaksson LA. 2001a. Cooperative effects by the initiation codon and its flanking regions on translation initiation. *Gene* **273**:259–265.
Stenström CM, Isaksson LA. 2002. Influences on translation initiation and early elongation by the messenger RNA region flanking the initiation codon at the 3' side. *Gene* **288**:1–8.
Stenström CM, Jin H, Major LL, Tate WP, Isaksson LA. 2001b. Codon bias at the 3'-side of the initiation codon is correlated with translation initiation efficiency in Escherichia coli. *Gene* **263**:273–284.
Stojković V, Fujimori DG. 2015. Radical SAM-Mediated Methylation of Ribosomal RNA. *Methods Enzymol* **560**:355–376.
Stojković V, Myasnikov AG, Young ID, Frost A, Fraser JS, Fujimori DG. 2020. Assessment of the nucleotide modifications in the high-resolution cryo-electron microscopy structure of the Escherichia coli 50S subunit. *Nucleic Acids Res* **48**:2723–2732.
Stojković V, Noda-Garcia L, Tawfik DS, Fujimori DG. 2016. Antibiotic resistance evolved via inactivation of a ribosomal RNA methylating enzyme. *Nucleic Acids Res* **44**:8897–8907.

Tenson T, Mankin A. 2006. Antibiotics and the ribosome. *Mol Microbiol* **59**:1664–1677.

Toh S-M, Xiong L, Arias CA, Villegas MV, Lolans K, Quinn J, Mankin AS. 2007. Acquisition of a natural resistance gene renders a clinical strain of methicillin-resistant Staphylococcus aureus resistant to the synthetic antibiotic linezolid. *Mol Microbiol* **64**:1506–1514.

Toh S-M, Xiong L, Bae T, Mankin AS. 2008. The methyltransferase YfgB/RlmN is responsible for modification of adenosine 2503 in 23S rRNA. *RNA* **14**:98–106.

Tu D, Blaha G, Moore PB, Steitz TA. 2005. Structures of MLSBK antibiotics bound to mutated large ribosomal subunits provide a structural explanation for resistance. *Cell* **121**:257–270.

Tuller T, Carmi A, Vestsigian K, Navon S, Dorfan Y, Zaborske J, Pan T, Dahan O, Furman I, Pilpel Y. 2010a. An evolutionarily conserved mechanism for controlling the efficiency of protein translation. *Cell* **141**:344–354.

Tuller T, Waldman YY, Kupiec M, Ruppin E. 2010b. Translation efficiency is determined by both codon bias and folding energy. *Proc Natl Acad Sci U S A* **107**:3645–3650.

Verma M, Choi J, Cottrell KA, Lavagnino Z, Thomas EN, Pavlovic-Djuranovic S, Szczesny P, Piston DW, Zaher HS, Puglisi JD, Djuranovic S. 2019. A short translational ramp determines the efficiency of protein synthesis. *Nat Commun* **10**:5774.

Vester B. 2018. The cfr and cfr-like multiple resistance genes. *Res Microbiol* **169**:61–66.

Vester B, Long KS. 2013. Antibiotic Resistance in Bacteria Caused by Modified Nucleosides in 23S Ribosomal RNA. Landes Bioscience.

Wellner A, Raitses Gurevich M, Tawfik DS. 2013. Mechanisms of protein sequence divergence and incompatibility. *PLoS Genet* **9**:e1003665.

Weßels C, Strommenger B, Klare I, Bender J, Messler S, Mattner F, Krakau M, Werner G, Layer F. 2018. Emergence and control of linezolid-resistant Staphylococcus epidermidis in an ICU of a German hospital. *J Antimicrob Chemother* **73**:1185–1193.

Wiegand I, Hilpert K, Hancock REW. 2008. Agar and broth dilution methods to determine the minimal inhibitory concentration (MIC) of antimicrobial substances. *Nat Protoc* **3**:163–175.

Wilson DN. 2014. Ribosome-targeting antibiotics and mechanisms of bacterial resistance. *Nat Rev Microbiol* **12**:35–48.

Wilson DN. 2009. The A–Z of bacterial translation inhibitors. *Critical Reviews in Biochemistry and Molecular Biology*. doi:10.3109/10409230903307311

Yan F, Fujimori DG. 2011. RNA methylation by radical SAM enzymes RlmN and Cfr proceeds via methylene transfer and hydride shift. *Proc Natl Acad Sci U S A* **108**:3930–3934.

Yan F, LaMarre JM, Röhrich R, Wiesner J, Jomaa H, Mankin AS, Fujimori DG. 2010. RlmN and Cfr are radical SAM enzymes involved in methylation of ribosomal RNA. *J Am Chem Soc* **132**:3953–3964.

Yang J, Zhang Y. 2015. I-TASSER server: new development for protein structure and function predictions. *Nucleic Acids Res* **43**:W174–81.

Zalucki YM, Power PM, Jennings MP. 2007. Selection for efficient translation initiation biases codon usage at second amino acid position in secretory proteins. *Nucleic Acids Res* **35**:5748–5754.

Zhang K. 2016. Gctf: Real-time CTF determination and correction. *J Struct Biol* **193**:1–12.

Zheng SQ, Palovcak E, Armache J-P, Verba KA, Cheng Y, Agard DA. 2017. MotionCor2: anisotropic correction of beam-induced motion for improved cryo-electron microscopy. *Nat Methods* **14**:331–332.

Zhou K, Zhou L, Lim Q 'en, Zou R, Stephanopoulos G, Too H-P. 2011. Novel reference genes for quantifying transcriptional responses of Escherichia coli to protein overexpression by quantitative PCR. *BMC Mol Biol* **12**:18.

Acknowledgements:

We thank members of the Fujimori lab for discussion and comments on the manuscript. We thank the UCSF Center for Advanced CryoEM, which is supported by the National Institutes of Health [S10OD020054 and 1S10OD021741] and the Howard Hughes Medical Institute (HHMI).

Funding:

NIAID R01AI137270 (DGF)

NSF GRFP 1650113 (KT)

UCSF Discovery Fellows program (KT)

NIGMS F32GM133129 (IDY)

NIGMS R01GM123159 (JSF)

Sangvhi-Agarwal Innovation Award (JSF)

Author contributions: KT conceived the research, designed and performed experiments, analyzed data, and wrote the manuscript. VS performed directed evolution, assisted in data interpretation, model refinement, and manuscript editing. LNG performed evolution experiments and manuscript editing. IDY and AGM performed structural analysis. JK and AP assisted in data acquisition and analysis. SNF provided data interpretation of polysome analysis and manuscript editing. AF, JSF, and DST assisted in experimental design, data interpretation, and manuscript editing. DGF conceived and supervised the research, assisted in data interpretation, and edited the manuscript.

Competing interests: Authors declare that they have no competing interests.

Data and materials availability: Atomic coordinates have been deposited in the Protein Data Bank under accession number 7LVK, and the density map has been deposited in the EMDB under accession number 23539.